MAY 1997 ECN-C--97-027

Final report of IEA Annex XIV : Field Rotor Aerodynamics

J.G. Schepers (Netherlands Energy Research Foundation)
A.J. Brand (Netherlands Energy Research Foundation)
A. Bruining (Delft University of Technology)
J.M.R. Graham (Imperial College)
M.M. Hand (National Renewable Energy Laboratory)
D.G. Infield (Rutherford Appleton Laboratory)
H.A. Madsen (Risø National Laboratory)
R.J.H. Paynter (Imperial College, Rutherford Appleton Laboratory)
D.A. Simms (National Renewable Energy Laboratory)

Acknowledgement

The support of the IEA R&D Wind Executive Committee which made it possible to cooperate in this Annex XIV is highly appreciated.

The measurement programme on the experimental facility of the Netherlands Energy Research Foundation was made possible by financial support from the Dutch Ministry of Economic Affairs (Energy R&D Targeted Funding 1991-1995).

The contribution from Risø to the IEA Annex XIV project has been funded by the Danish Ministry of Energy under contract: ENS 1364/94-0001 which is gratefully acknowledged.

The U. S. Department of Energy is credited for its funding of the Unsteady Aerodynamics test program through the National Renewable Energy Laboratory under contract number DE-AC36-83CH10093.

The measurement programme from Imperial College/Rutherford Appleton Laboratories was funded by the Department of Trade and Industry, Energy Technology Support Unit and Engineering and Physical Sciences Research Council.

Furthermore the European experimental programmes were funded through several JOULE projects. These JOULE projects are partly funded by the EU and partly by the participating organisations and/or their national agencies.

Abstract

This report describes the work performed within the IEA Annex XIV 'Field Rotor Aerodynamics'.

In this Annex five organisations from four countries collaborated in performing aerodynamic experimental programs on full scale horizontal axis wind turbines at field conditions. In these experimental programs local aerodynamic quantities (forces, velocities) are measured at several locations along a rotor blade.

The following organisations (and persons) cooperated in the projects:

- Netherlands Energy Research Foundation (ECN, NL) (Operating Agent) J.G. Schepers, A.J. Brand;
- Delft University of Technology (DUT, NL): A. Bruining
- Imperial College (IC, UK), together with Rutherford Appleton Laboratory (RAL, UK): J.M.R. Graham, D.G. Infield, R.J.H Paynter
- National Renewable Energy Laboratory (NREL, USA): D.A. Simms, M.M. Hand
- Risø National Laboratory (Risø, DK): H.A. Madsen

As a result of the international collaboration within IEA Annex XIV it has been possible to coordinate data processing and to create a database of measured data from all participants in a common file format. The database is stored on CD-ROM or accessable through anonymous ftp.

The detailed aerodynamic measurements obtained on very different turbines, give a unique opportunity to better understand the aerodynamic behaviour of a wind turbine. This may result in the development and validation of more accurate aerodynamic models.

Special attention is paid to the definition of the angle of attack and the dynamic pressure at rotating wind turbine experiments. The definition of these quantities

is less straightforward than in the case of a wind tunnel environment.

Keywords

Horizontal Axis Wind Turbine Aerodynamics

Full scale aerodynamic experiments

SUMMARY

This report describes the work and the results of 'IEA Annex XIV: Field Rotor Aerodynamics'.

The objective of the Annex was defined as the coordination of full scale aerodynamic test programs on wind turbines, in order to acquire the maximum of experimental data at minimum costs. In these full scale aerodynamic test programs local aerodynamic quantities (forces, inflow velocities, inflow angles) are measured at several radial positions along the blade. The supply of local aerodynamic data, is a major step forward in understanding the very complicated aerodynamic behaviour of a wind turbine. In conventional test programs only blade (or rotor) quantities are measured. Usually these quantities are integrated over the rotor blade(s) and they are not only influenced by aerodynamic effects, but also by mass effects. Then the local aerodynamic properties of the blade can only be derived indirectly, introducing an uncertainty.

A total of five full scale aerodynamic test programs were coordinated. The programs were carried out by:

1. Delft University of Technology, DUT Netherlands: The DUT experiments are carried out on a 2 bladed, 10 m diameter turbine. The blades are untwisted and untapered.
2. Imperial College, IC and Rutherford Appleton Laboratory, RAL, United Kingdom: The IC/RAL experiments are carried out on a 3 bladed, 16.9 m diameter turbine. The blades are twisted and tapered.
3. Netherlands Energy Research Foundation, ECN, Netherlands (Operating Agent): The ECN experiments are carried out on a 2 bladed, 27.4 m diameter turbine. The blades are twisted and tapered.
4. National Renewable Energy Laboratory, NREL, USA: The NREL experiments are carried out on a 3 bladed, 10 m diameter turbine. Measurements on two types of blades have been supplied:
   - An untwisted and untapered blade;
   - A similar blade, without taper, but with twist.
5. RISØ National Laboratory, Denmark: The RISØ experiments are carried out on a 3 bladed, 19 m diameter turbine. The blades are twisted and tapered.

By the coordination of the test programs it has been possible to create a well documented base of experimental data. The base provides unique aerodynamic data for very different wind turbine configurations which can provide a better understanding of the aerodynamic behaviour of a wind turbine. As a result more accurate aerodynamic models can be developed and validated.

In order to create the database, a joint measurement program was agreed upon. It was agreed that measurements should be supplied in which the angle of attack ranges from negative values to deep stall values. Also measurements at yaw misalignment and at stand still have been supplied. The data file formats and the conventions have been harmonized in order to make the database easily accessible. To aid in the interpretation of the data, an aeroelastic model description is made of all facilities.

Some recommendations were defined at the end of the project:

- The largest turbine in the project has a diameter of 27.4 m. Although at the start of the project, this was considered to be a medium sized turbine, it was regarded a relatively small turbine at the end of the project. Aerodynamic measurements on larger turbines would be very useful.
- The mutual comparison of the measurements in the database is complicated by the fact that the angle of attack and dynamic pressure were manipulated differently by the participants. These properties are defined less straightforwardly than in the case of wind tunnel measurements. Although the project results indicate that the mean angle of attack and dynamic pressure which result from the different methods yield a reasonable mutual agreement, the differences in standard deviations are considerable and more investigation on this subject is required.
- There is a clear need for maintenance of the database. By maintaining the database an extensive use of the database can be expected, not only in the near future, but also on the long term.

CONTENTS

1. INTRODUCTION

This report describes the work which was performed in IEA Annex XIV 'Field Rotor Aerodynamics'. In this Annex the following institutes participated:

- Delft University of Technology, DUT Netherlands
- Imperial College, IC and Rutherford Appleton Laboratory, RAL, United Kingdom
- National Renewable Energy Laboratory, NREL, USA
- Netherlands Energy Research Foundation, ECN, Netherlands (Operating Agent)
- RISØ National Laboratory, Denmark

All these institutes have experimental facilities at which detailed aerodynamic measurements are performed on full scale horizontal axis wind turbines. These measurements aim at a better understanding of the aerodynamic behaviour of a wind turbine. A better understanding is required because the prediction of wind turbine aerodynamics is a very complex task. Several aerodynamic phenomena, like (steady and unsteady) stall, dynamic inflow, tower effects, yaw effects etc. contribute to unknown aerodynamic responses. These unknown responses make it very difficult to design cost-effective and reliable wind turbines. Turbines behave unexpectedly, experiencing instabilities, power overshoots, or higher loads than expected.

In conventional experimental programmes the behaviour of a turbine is analysed by means of measurements of integrated, total (blade or rotor) loads. These loads consist of an aerodynamic and a mass induced component and are integrated over a certain spanwise length. This gives only indirect information about the aerodynamics at blade element level. At the end of the 80's the insight grew that direct measurements of aerodynamic properties relevant for dynamic load codes (i.e. lift, drag and moment coefficients, inflow angle, inflow velocity at several radial positions) were needed. As a result the participants of IEA Annex XIV initiated the construction of full scale aerodynamic test facilities at which these properties can be measured.

However, such aerodynamic field experiments are typically very time consuming, expensive and complicated through the large volumes of data and the extensive data reduction which are required. Furthermore, each turbine configuraton that is investigated experimentally may exhibit a very different aerodynamic response characteristic. Hence, the results which are obtained from the very time consuming, expensive and complicated experiments may have only a limited validity.

For this reason it was considered very advantageous to cooperate in these experiments. This cooperation is established in the IEA Annex XIV 'Field Rotor Aerodynamics' which commenced in 1992.

The cooperation enabled the creation of an extensive database of aerodynamic measurements. This base provides unique aerodynamic data for a large number of wind turbine configurations, which can be used for model validation and model development. The resulting insights and models will have more general validity than those obtained from the experimental programs independantly.

Furthermore, the project served as a platform where very specific knowledge associated with aerodynamic measurements could be exchanged. This has been very instructive for all participants by which the experimental programs could be accelarated.

In this final report, several items are adressed:

- The objective of the project is described in chapter 2.
- The workprocedure is described in chapter 3.
- A description of all experimental facilities, including the measurement procedure is given in section 4. The description of the facilities is supplied by the participants. All contributions cover similar topics, but there are some differences in the degree of detail. A detailed aeroelastic description of all turbines involved in IEA Annex XIV is presented in Appendix C to Appendix G.
- When applying the results of the database, it should be realised that the mutual comparison of measurements from the base is complicated by the fact that the angle of attack and the dynamic pressures have been manipulated differently by the several participants. This issue is addressed in the chapters 5 and 6.
- A global description of the database is given in chapter 7. The harmonisation which had to take place in order to allow the user an easy access to the base is also described in this section. Among others, the file formats, the file types and the file names are explained. The prescribed conventions and notations are given in Appendix A. Note that, unless otherwise stated, these conventions and notations have been applied throughout the present report too.
- The conclusions and recommendations which result from the project are presented in chapter 8.

2. OBJECTIVE OF IEA ANNEX XIV

The objective of the IEA Annex XIV has been defined as the coordination of measuring programmes on the field rotor aerodynamic facilities of the participants in order to acquire the maximum of experimental data at minimum costs. As a result of the project, a base of experimental data should be created which serves as a basis for:

- the validation and development of design codes and
- the design of stall controlled turbines.

Although the main objective of IEA Annex XIV has been on the field of stall aerodynamics, the database of experimental data is also useful for many other purposes. Among others the aerodynamics of 'pre-stall' conditions, parked conditions, tower shadow and yaw misalignment is measured.

3. WORK PROCEDURE

The main objective of the IEA Annex was to create an organized database of detailed aerodynamic measurements on several wind turbine configurations. In order to reach the objective, a number of different tasks were distinguished, which are listed below.

3.1 Definition of test matrix

In the initial phase of the IEA Annex, the parties reached consensus about a joint program of measurements. The test matrix given below served as a guideline for the selection of measurements to be supplied in the database.

	Re *) (-)	α_{mean} $(^o)$	yaw angle $(^o)$
ECN	1.8 10^6	-5 to + 40	$\pm$ 30 à 40
DUT	0.9 10^6	-5 to + 40	$\pm$ 30 à 40
NREL	0.7 10^6	-5 to + 40	$\pm$ 30 à 40
IC/RAL	1.0 10^6	-5 to + 40	
RISØ	1.0 10^6	-5 to + 40	$\pm$ 30 à 40

*) Reynolds number at rotating conditions at 70% R;

It was agreed that rotating measurements should be supplied for:
- Mean yaw angle $\approx$ zero. This yields a more or less constant angle of attack.
- Mean yaw angle $\neq$ zero; In these campaigns the angle of attack variations are deliberately triggered.

Note that it was intended to supply measurements with pitch variations too. These measurements could be supplied by ECN and NREL. Within the course of the project the priority of these measurements was downgraded and in order to limit the amount of work these measurements were skipped.

At a later stage of the IEA Annex it was agreed that, apart from rotating measurements some parties would also supply measurements for non-rotating conditions.

3.2 Conventions and notations

To interpret the measurements it was considered extremely useful to have agreement on the conventions and notations. To this end a document was prepared which describes the conventions and notations. The document is annexed in Appendix A. It originates from the document which was prepared for the JOULE projects 'Dynamic Inflow', [1]. Special attention was paid to the rotational direction of the turbines. Most (but not all) of the turbines in the project rotated counter-clockwise (looking downwind to the rotor). This complicates the mutual comparison of results in particular under yawed conditions. For this reason some coordinate systems were transformed such that a mutual comparison of results was possible. The conventions and notations from Annex XIV were also used as a basis for the conventions to be used in the JOULE project 'Dynamic Stall And Three Dimensional Effects', [2].

3.3 Format of the files, filetypes, filenames

In order to facilitate the selection of signals from a file, it was considered essential that all files were supplied in the same format. Also the file names and file types were harmonized. This item is further discussed in section 7.

It turned out that the large datafiles led to a 'psychological barrier' for potential users. This was mainly caused by the decision to exchange files which contain a huge amount of measured information, although in most cases only a selection of the data is required. However, it was considered impractical to prepare specific data files for different users. Therefore much effort was spent on the agreement of a common format and common conventions and the documentation of the database. This includes statistical overviews and time traces plots of every file. This made it possible for all users to extract the relevant information in a relatively convenient way.

3.4 Selection of campaigns

In order to fill out the test matrix, campaigns were selected on basis of statistical data (mean values, minimum values, maximum values and standard deviations) of a selected number of signals.

3.5 Supply, storage and documentation of data files

The data is stored on a public ECN disc and on CD-ROM. Several data exchange rounds appeared to be necessary before a satisfactory result was achieved. The participants are able to retrieve data from the ftp site by anonymous ftp. The content of the database was documented by means of status reports. In these reports, the format of every file was documented together with the statistical overviews of the several campaigns, see Appendix B.

3.6 Machine data report

For the interpretation of the measured data it was considered useful to have the availability of the aerodynamic, geometric and elastic data of all the facilities which are involved in the project. Therefore a questionnaire was made which specifies the machine data of all the turbines which are involved in the project. The results are reported in Appendix C to Appendix G.

3.7 Angle of attack report

One of the main problems in aerodynamic field experiments is the definition of the angle of attack. In wind tunnel experiments, the angle of attack is easily known from the wind tunnel set angle. However in rotating conditions such an angle is not known. Often the angle of attack is measured with a flow sensor some distance ahead of the blade element. This angle however cannot be translated straightforward to an equivalent wind tunnel angle of attack and corrections have to be applied. These corrections are different for every participant. Other participants derived the angle of attack from the pressure distribution. Consequently the comparison of the measurements from the different participants may be obscured by differences in the definition of the angle of attack.

Within the course of the project, a discussion document about this subject has been prepared by ECN. This document served as food for discussion at several meetings. This issue is further adressed in section 5

3.8 Meetings

A total of 7 meetings (including a preparatory meeting) have been held which were attended by all the institutes who were involved in the Annex. The meetings were always held at the institutes and a visit to the experimental facilities was one of the agenda points.

Detailed minutes of every meeting were prepared.

- A preparatory meeting was held at the Delft University of Technology on December 2nd 1992, see [3]. At this meeting agreement was reached on the workplan.
- The first meeting was held at RISØ National Laboratory on September 16th and 17th, 1993, see [4]. At this meeting a large number of technical aspects (a.o. the length of time series, scan frequency, definition of the angle of attack) and the problem of the selection of the most suitable datafiles was adressed.
- The second meeting was held at the University of Delft on March 17th and 18th 1994, see [5]. At this meeting a further discussion took place of the technical points which are mentioned at the second meeting. Furthermore a selection was made of the most suitable datafiles from NREL, RISØ and DUT.
- Subsequently, the IEA Annex XIV project became closely related to the EU JOULE project 'Dynamic Stall and 3D effects', [2]. All institutes which participate in the IEA Annex were involved in the JOULE project as well and attended the project meetings of the JOULE project. For this reason no separate IEA Annex XIV meetings were held until April 5th 1995 at Rutherford Appleton Laboratory, see [6]. At this third meeting the main discussion point was the problem of the large datafiles which in the JOULE project has led to a 'psychological barrier' for potential users of the database. It was decided that even more emphasis should be put to the precise documentation of the format of the datafiles, by which the selection of the desired signals is relatively easy.
- A fourth meeting was held at NREL on February 5^{th} and 6^{th} 1996, see [7]. Between the third and the fourth meeting some of the measurement programs were accelerated considerably and much new data have been presented. Much attention was paid to the discussion document on the angle of attack.
- A fifth meeting was held at ECN on June 14^{th} 1996, see [8]. Again a considerable amount of new data was presented. In addition, the content of the final report was discussed in some detail.
- The sixth meeting was held at RISØ on February 20 and 21 1997. At that time a draft of the final report was available, which was discussed extensively. Also a proposal for an extension was discussed.

4. DESCRIPTION OF EXPERIMENTAL FACILITES

4.1 ECN test turbine

4.1.1 Introduction

The aerodynamic experiments at ECN were performed in two different phases:

- The non-rotating phase (1993-1994): In this phase the blade was mounted vertically on a non-rotating facility in the free stream. This test aimed at acquiring data at free stream conditions without rotational effects. Furthermore the instrumentation could be tested relatively easy in order to prepare for the next phase:
- The rotating phase (1995-1997). In this phase the blade was mounted on the HAT-25 experimental wind turbine and data were acquired under rotation. Furthermore some non-rotating measurements have been repeated. In this report the measurements from the rotating phase are reported only.

More information on the facility can be found in [9] and [10].

4.1.2 Global characteristics of facility

- Blade: Aerpac 25 WPX blade mounted on the HAT-25 experimental wind turbine, see figure 4.1.
- Number of blades: 2
- Blade span (from flange to tip) = 12.1 m
- Rotor diameter = 27.44 m
- Blade profile: NACA44xx
- Blade with twist and taper: Twist $\approx$ 12 degrees, root chord = 1.5 m, tip chord = 0.412 m.
- Pressure tap measurements around profiles at 3 different radial stations, see figure 4.2.
- Inflow angle and inflow velocity measured at inboard station with 5 hole probe, see figure 4.2.

Location

The HAT-25 wind turbine is located at ECN near Petten in the Netherlands. Figure 4.3 gives a picture of the site. The prevailing wind direction is from South-West, at which most of the measurements are taken. In this direction, the terrain upstream of the turbine is obscured by dunes over around 600 m. As a result, the turbulence intensities at the site may depend strongly on the conditions. Generally, the values of the turbulence intensities are between 5% and 20%.

4.1.3 Instrumentation

Blade instrumentation:

- Pressure taps at 3 rotor blade sections, see [9].
  These taps are positioned at 36%, 64% and 82% of the rotor radius.
  All 3 sections are measured simultaneously:
  There are 47 taps per station, see figure 4.4.
  Extreme care was taken to manufacture taps with a surface roughness of the order of the one of the rotor blade (10 μm). The diameter of a pressure tap is

Figure 4.1 *ECN test facility*

1mm. A so called minitube connects a pressure tap to a pressure transducer. Each minitube is mounted perpendicular and flush to the local rotor blade surface. The length of all minitubes is 1.1 m and their internal diameter is 1 mm. For this kind of tubes it has been found experimentally that acoustic damping is small for frequencies up to 40 Hz, [11]. The pressures at the surface of the blade are measured with the Scannivalve Hyscan 2000 system, which has a scan rate up to 100 kHz. A total of 9 Scanivalve ZOC-14 pressure scanners are used to measure these blade pressures. 5 Scanivalve ZOC-14 pressure scanners have a full-scale range of about 2.5 kPa (30% station, and pressure sides of the 60% station and the 80% station), 2 Scanivalve ZOC-14's have a range of about 5 kPa (suction side of the 60% station), and 2 Scanivalve ZOC-14's have a range of about 12 kPa (suction side of the 80% station). The absolute error of the scanners is about 5.0 Pa, 7.5 Pa and 5.6 Pa, respectively. The ZOC-14 modules are mounted inside the rotor blade. Six modules (those of the 30% and the 60% station) are operating in a thermally

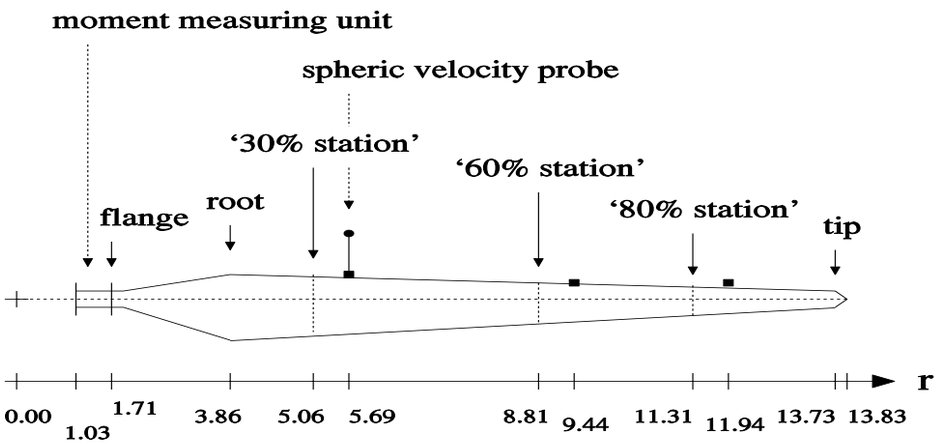

Figure 4.2 *Instrumentation of ECN blade*

controlled environment (Scanivalve TCU) and three modules (the ones at the 80% station) are mounted on a heating element in order to minimise temperature differences. For calibration, a pressure generator (Scanivalve Calmod 2000) in combination with a secondary standard (Mensor Model 11603) is used, see below.

For each station the 48th sensor is short-circuited, which means the measuring side of the sensor is connected to the reference side of the sensor. (The other 47 sensors are connected to the 47 taps.) As a result, the pressure reading of this sensor should be zero. If this reading is not zero, an error in the Hyscan system may have occurred. Inspection of the pressure readings from a short-circuited sensor thus allows for an assessment of the quality of the measured pressure data.

An automatic purge option was available.

The pressures are measured relative to an unknown reference pressure. The pressure inside the blade near the hub is used as reference.

- Spheric velocity probe: The magnitude and the direction of the flow towards a rotor blade section is measured with a spheric velocity probe. A spheric velocity probe consists of a sphere and a rod (figure 4.5). The sphere contains the pressure taps and the pressure sensors. The cylindrical rod connects the sphere to the leading edge of the rotor blade.

  At the surface of the sphere five pressure taps are located: one centre tap and two pairs of symmetrically opposite taps (figure 4.6). The centre tap is located on the x axis of the sphere. The two pairs of taps are in two perpendicular planes; the position of a tap in a plane is given by the base angle. (The base angle is the angle between the tap and the centre tap.) For a spheric probe to work well it is essential that the centre hole is on the x axis and the four base angles are equal. The specifications for a spheric probe are described separately [12].

  The pressure difference between the absolute pressure in a tap and a reference pressure is measured by a Scanivalve ZOC23 pressure sensor with a range of

Figure 4.3 *The site where the HAT-25 experimental wind turbine is located. Also indicated is the mast where wind speed and wind direction are measured*

about 2.5 kPa and an absolute error of about 5 Pa. This sensor is mounted inside the sphere and connected to the Hyscan 2000 system. The ZOC23 module is *not* operating in a thermally controlled environment. In order to mimimise temperature differences, foam (Neoprene) was put into the sphere. In addition, a platinum resistance thermometer element (Rössel RL-4330/1-B-1) was mounted on the ZOC23 module so that temperature changes can be monitored. The output of this thermometer element was connected to the Hyscan 2000 system via the Scanivalve EIM, see below. The relation between AD counts and engineering units was determined by calibration; the corresponding calibration coefficients were included in the 'initfile' of the data processing.

The layout of the eight sensors of the ZOC23 module is as follows: three sensors are connected to each of tap #1, #2 and #3; two sensors are connected to tap #4; two sensors are connected to tap #5; and one sensor is connected to the reference. This layout ensures two pressure readings are available from the taps which are most sensitive to changes in the angle of attack. (In the analyses of the current field measurements the computation of the probe inflow velocity and direction was however based on one reading only.) In addition, it ensures a short-circuited pressure sensor is available, which allows for an inspection of the quality of the data.

The sphere has a diameter of 58 mm and the base angle of the pressure taps is 14.8^o. The rod has a length of 1.07 m and is mounted at a radial position

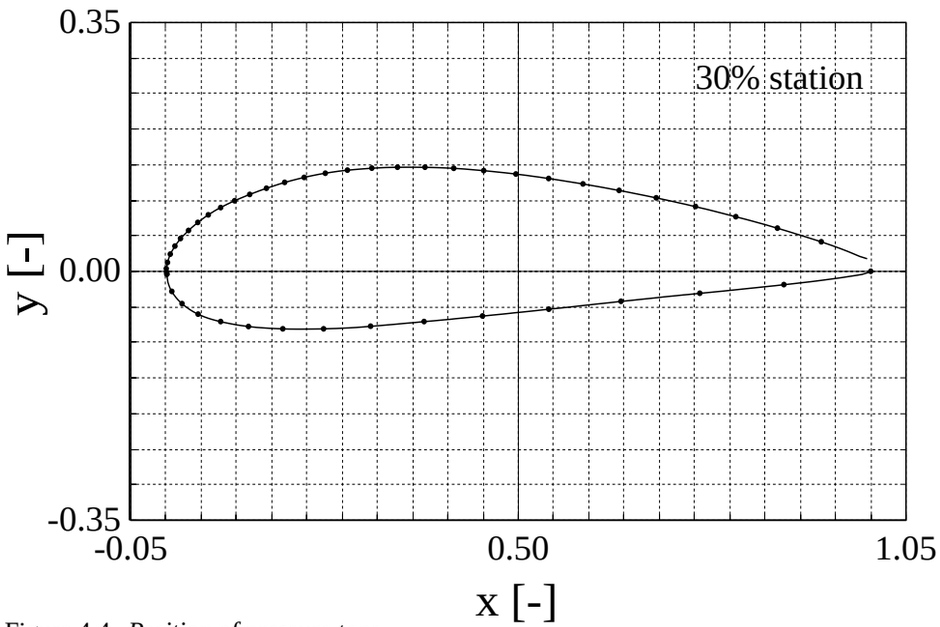

Figure 4.4 *Position of pressure taps*

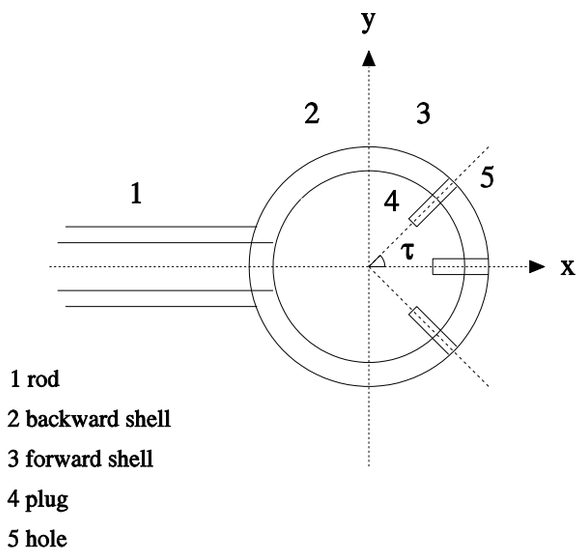

Figure 4.5 *A schematic of the spheric probe. Indicated is the base angle τ.*

r =5.69 m (42% of the rotor radius; 35% station). It is oriented at 13.5° to the chord and at 3.0° to the cross-section of this station; the probe axis crosses the local chord at $x/c = 0$. Figure 4.7 shows a schematic of the spheric velocity probe at the 35% station of the rotor blade. The construction, calibration and data handling of this probe are described separately, see [13].

Additional signals

- Wind turbine signals
  - Nacelle orientation
  - Rotor speed
  - Rotor azimuth

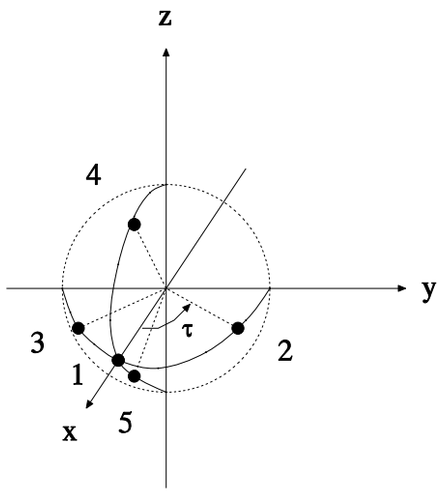

Figure 4.6 *The location of the pressure taps at the surface of the sphere of the spheric probe. Indicated is the base angle τ.*

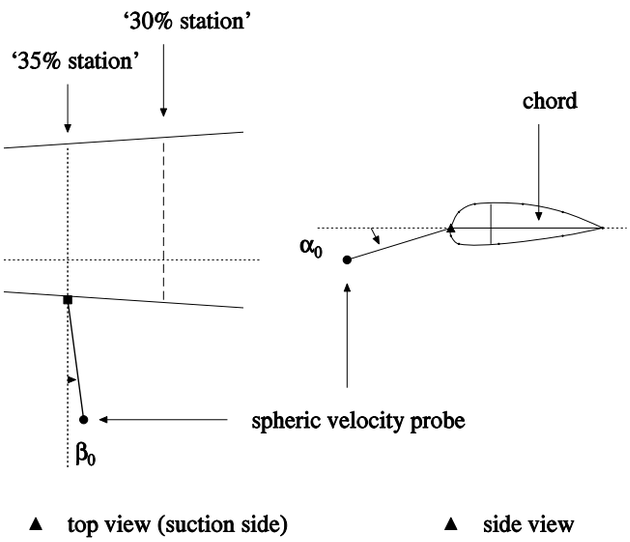

Figure 4.7 *The location of the spheric velocity probe at the 35% station. Indicated are the probe orientation angles $\alpha_0 = 13.5^o$ and $\beta_0 = 3^o$.*

  - Blade pitch angles
  - Rotor shaft torque
  - Axial force on the rotor
  - Root lead-lag bending moments
  - Root flap bending moments

- Ambient conditions
  - Wind speed at three heights:
    - V_{hub}; Ambient wind speed at hub height;
    - V_{up}; Ambient wind speed at h = hub height + 10 m;
    - V_{low}; Ambient wind speed at h = hub height - 10 m;

The wind speeds are measured with mast B which is indicated in figure 4.3
- Wind direction at h = hub height + 10 m
- Atmospheric pressure
- Air temperature

Measurement system components

A detailed description of the instrumentation is given in [9] and [10]. As stated above, the aerodynamic measurement system is based on the Scannivalve's Hyscan system.

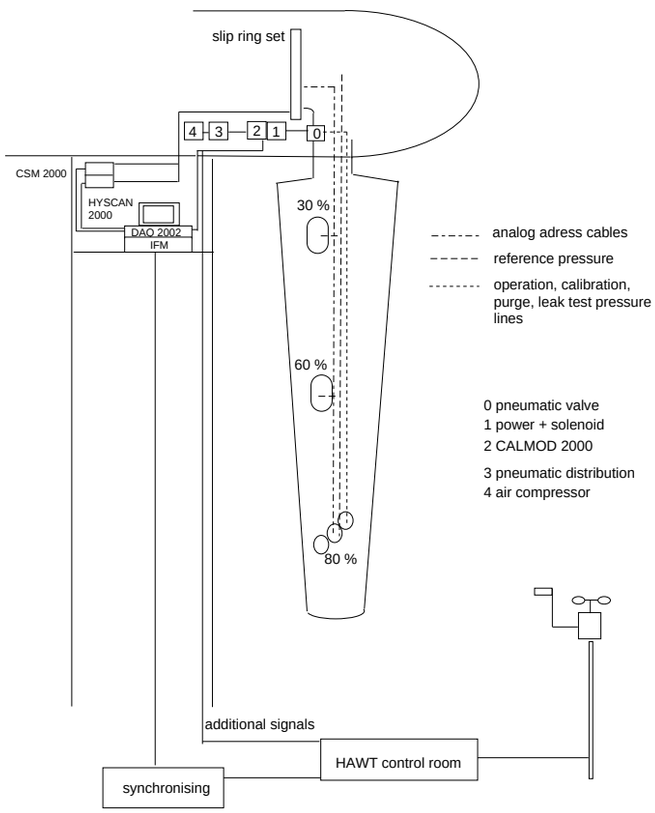

Figure 4.8 *ECN: Measurement system*

Apart from the pressure scanners this system consists of (see also figure 4.8):
- DAQ2002 data acquisition system.
  The DAQ2002 is a self contained, PC based, high speed data acquisition system. Measurements are conditionally stored on the hard disc of the PC and then transmitted to the host computer. The PC is located on a platform approximately 3 metres below the rotor axis.
- IFM 2000
  The IFM 2000 is required when using ZOC modules with the HYSCAN system. It is an interface module that contains: line drivers and addressing circuitry, the frame list memory, multiplexers and amplifiers, interval times and A/D clock logic.
- CALSYS 2000 Calibration system:

This system consists of the CALMOD 2000 Calibrator Modules and the PSC 2000 Power Solenoid Conrol Module.
The CALMOD 2000 is designed to generate known pressures for individual pressure sensor correction. The CALMOD 2000 can perform quick or full calibrations: Zero calibration, 4 point positive calibration, 4 point negative calibration, or a full 7 point calibration. This calibration system operateas in a closed loop routine with the DAQ 2002 yielding minimum calibration times, system leak detection, and data reliability.
The CALMOD 2000 is placed in the nacelle of the turbine. The ZOC modules in the blade are accessable via a pressure valve which is mounted close to the root of the blade. The test sessions include calibration sequenses when the turbine in stopped. With the aid of the pressure valve, the CALMOD 2000 is adapted to the ZOC modules.
The PSC 2000 Power Solenoid Control Unit provides 24 volt power for the calibrator modules and the solenoids for the ZOC calibration valves. The PSC 2000 also allows pneumatic control to ZOC modules.

- CSM 2000 Cable Service Unit:
  The CSM 2000 is used to service the ZOC modules. The CSM 2000 provides DC power and can support a maximum of 8 ZOC electronic pressure scanners. The CSM receives address information from the IFM 2000 and distributes it to the ZOC modules. It also returns the analog signals from the ZOC modules to the IFM 2000. A built in power supply provides +/- 15 VDC power to the modules.

The data acquisition system for the additional signals is located in the HAT control room, see figure 4.3. The aerodynamic measurements and the measurements of the additional signals are synchronised, so that they can be merged.

Transfer of all rotor signals is achieved through slip-rings.

4.1.4 Measurement speed

All data channels which originate from the Hyscan system are sampled with 128 Hz or 64 Hz effectively. The additional signals are sampled with 64 Hz or 8 Hz and oversampled to 128 Hz or 64 Hz, whichever needed.

4.1.5 Data reduction

Pre-processing of acquired data:

- Three-point median filter, and
- First-order Butterworth filter
  (bandwidth 10 Hz)

The effect of filtering is illustrated in figure 4.9 and 4.10.

For each station the measured pressure differences are reduced to

- Pressure distributions,
- Normal forces per unit length,
- Tangential forces per unit length,
- Inflow velocities, and
- Angles of attack.

For the velocity probe the measured pressure differences are reduced to

- Inflow velocities,
- Angles of attack, and

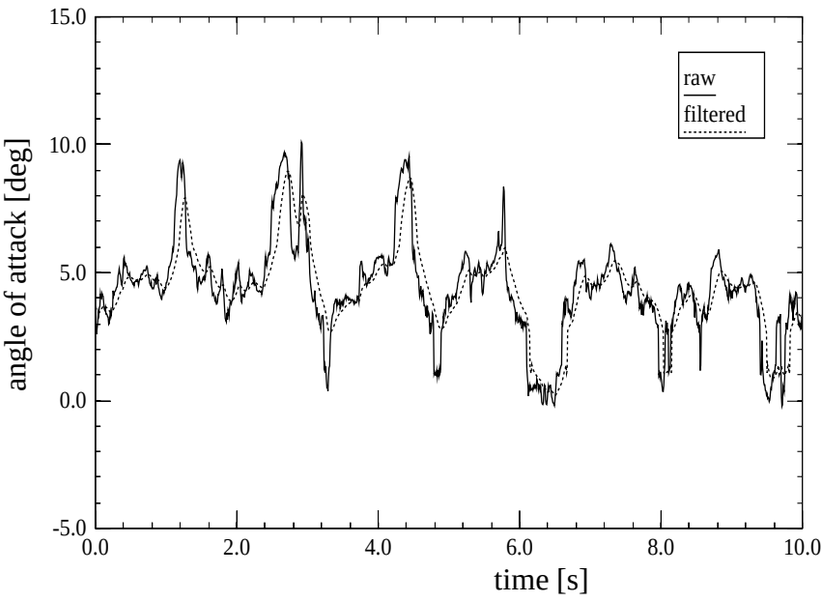

Figure 4.9 *ECN: The effect of applying the filter seen on a time trace of the measured angle of attack*

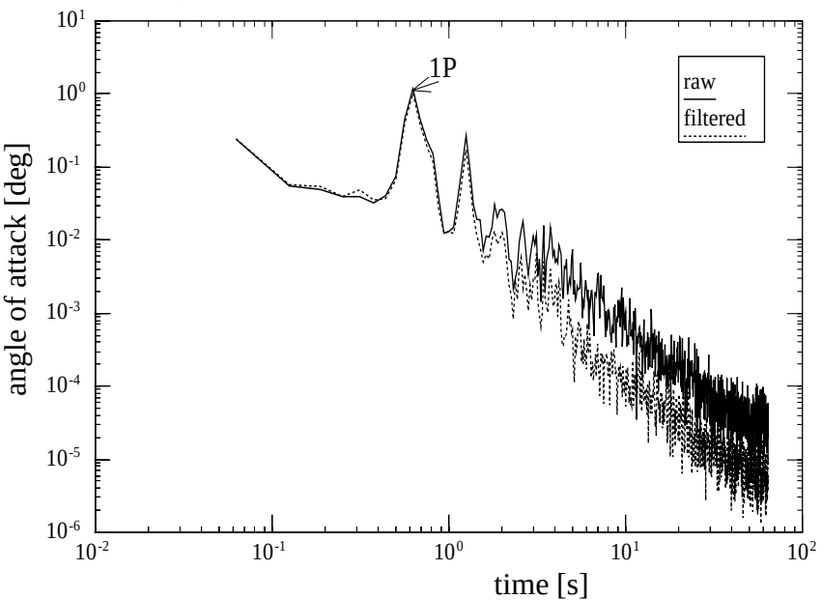

Figure 4.10 *ECN: The effect of applying the filter seen on a power spectrum of the measured angle of attack*

- Cross-flow angles.

Pressure distribution

$p'_j \equiv p_j - p_{ref}$ = pressure difference measured in the jth pressure tap.

$p'_{j,cor} \equiv p'_j + p_{cent}$ = compensated pressure difference, i.e. the pressure difference in the jth tap compensated for the pressure due to the centrifugal force

$$p_{cent} = p_a \left(\exp\left(\frac{\rho\Omega^2}{2p_a}(r_t^2 - r_m^2) \right) - \exp\left(\frac{\rho\Omega^2}{2p_a}(r_r^2 - r_m^2) \right) \right),$$

ρ = air density,
r_t = radial position of tap,

r_m = radial position of sensor membrane,
r_r = radial position of the entrance to reference tube.

Pressure coefficient

$$c_{p,j} \equiv \frac{p'_{j,cor}}{p'_{ST,cor}},$$

$p'_{ST,cor}$ = stagnation pressure
(i.e. the largest positive pressure difference in the compensated pressure distribution).

Normal force per unit length:

$$n = \sum_{j=PS} p'_{j,cor} x'_j c - \sum_{j=SS} p'_{j,cor} x'_j c,$$

x'_j = non-dimensional length corresponding to the jth pressure tap,
c = chord length.

Normal force coefficient:

$$c_n \equiv \frac{n}{p'_{ST,cor} c}.$$

Tangential force per unit length:

$$t = \sum_{j=LE} p'_{j,cor} y'_j c - \sum_{j=TE} p'_{j,cor} y'_j c,$$

y'_j = non-dimensional length corresponding to the jth pressure tap.

Tangential force coefficient:

$$c_t \equiv \frac{t}{p'_{ST,cor} c}.$$

Stagnation angle of attack:
Direction of the flow towards an airfoil section is obtained from the position (x_{ST}, y_{ST}) of the stagnation point on the airfoil surface

$$\alpha_{ST} = \arctan\left(\frac{-y_{ST}}{x_M - x_{ST}}\right) + c_0 + c_1 x_{ST},$$

calibrated against pressure distributions measured in a windtunnel.

Error analysis on stagnation angle of attack on basis of a windtunnel calibration

$$\begin{aligned} \Delta\alpha_{ST} &\leq 1\ ^{\circ} \quad \text{for} \quad \alpha_{ST} \leq 10\ ^{\circ} \\ \Delta\alpha_{ST} &\leq 2\ ^{\circ} \quad \text{for} \quad 10\ ^{\circ} < \alpha_{ST} \leq 30\ ^{\circ}. \end{aligned}$$

Inflow velocity:
The inflow velocity is the characteristic value of the speed of the flow towards a rotor blade section, which is obtained from the stagnation pressure:

$$U_{ST} \equiv \sqrt{\frac{2p'_{ST,cor}}{\rho}}.$$

Probe inflow velocity and probe angle of attack:
The magnitude and direction of the flow towards the spheric velocity probe in terms of

- Probe inflow velocity U_p,
- Probe angle of attack α_p, and
- Probe cross-flow angle β_p;

which are obtained by iteratively solving an estimative relation based on inviscid flow theory (no upwash correction).

Error analysis on probe inflow velocity and angle of attack On basis of a wind tunnel calibration:

$\Delta U_p = 0.4$ m/s at $U_p = 10$ m/s and
$\Delta U_p = 1.0$ m/s at $U_p = 35$ m/s;

$\Delta\alpha_p \leq 2.5^\circ$ for $0^\circ \leq \alpha_p \leq 30^\circ$ at $U_p = 10$ m/s and
$\Delta\alpha_p \leq 1.5^\circ$ for $0^\circ \leq \alpha_p \leq 30^\circ$ at $U_p = 35$ m/s.

4.2 IC/RAL test turbine

4.2.1 Global characteristics of facility

- Blade: LM - 8.5 blade mounted on a Windharvester wind turbine.
- Number of blades: 3
- Blade span (from flange to tip) = 8.2 m
- Rotor diameter = 17 m
- Blade profile: NACA632xxx
- Blade with twist and taper: Twist = 15 degrees, root chord = 1.09 m, tip chord = 0.445 m.
- Pressure tap measurements around profiles at 6 different radial stations, see figure 4.11.
- Inflow angle and inflow velocity is measured on 3 locations with 5 hole pitot probes, see figure 4.11 and 4.12.

Figure 4.11 *Instrumentation of IC/RAL blade*

Location

The experimental facility is located at the Rutherford Appleton Laboratory's wind site, about 80 km West of London: The Laboratory is set on a plateau to the north of a range of hills called The Ridgeway. From the turbine position (the base has an altitude of 135.82m) the following features may influence the wind:

- N to NE: Mix height buildings, the nearest large building being 20m high, 200m away

- East: A smooth grassed mound summit 150m about 150m away
- SE to W: Gentle gradient open farmland, the Ridgeway running East to West has a maximum altitude of about 220m, 1.5km away
- W to NW: Small woodland (about 300m away) with a low cropped field close to the turbine.

The prevailing winds are from the Southwest with an annual mean of about 4.5m/s and typically 17for the roughness is 0.03m.

4.2.2 Instrumentation

Briefly the instrumentation system consists of two loggers: One is situated in the hub, collecting data from the rotor, another logger collects data from ground fixed transducers. There is a communication link to allow remote control and file transfer with the hub based logger. The data from the loggers is synchronised with a pulse stream so that the separate data files can be merged together.

Hub mounted PC-based logger

The decision to mount a logger in the hub was made to reduce the need for a large number of slip-rings - about 40 tracks would have been needed - instead only: power, a communication link and a synchronisation pulse is needed.

The logger is based on an IBM-PC compatible passive backplane and has five boards:

- CPU and RAM (386-33 MHz and 16 MByte). The reasonably large memory allows temporary storage of up to about 7 Million samples in a 'RAM-disk'.
- Floppy disk emulator (1.44 MB ROM, 1.44 MB SRAM). The floppy disk emulator means the system has no moving parts and is sufficient to store control programs and the operating system.
- Serial communications (RS422, 288 kbaud). The communication allow a remote terminal and file transfer including programs and data from another PC.
- Video adapter. This allows bench use during development.
- Data acquisition and Control (14-bit, 16 channel, 100 ksamples/sec, five 16 bit counters). This collects data and provides control signals to the system of transducers.

Blade instrumentation

A new blade was purchased from LM Glasfiber, the manufacturer, into which the instrumentation has been installed. The main data comes from about 180 tappings on the blade, these are distributed as follows, see figure 4.11

- Six stations along the blade each with 26 tappings: The stations are arranged approximately square to the leading edge at 20%, 30%, 40%, 50%, 65% and 80% radius. There is a greater concentration of holes near the leading edge where the larger pressure gradients are found.
- Three inflow speed and direction probes: These are five hole Pitot probes mounted to protrude from the upwind side of the blade so that the point is about two-thirds of a chord ahead of the blade. The probes are 25 mm diameter with a hemispherical head with five tappings (one central and four at a 45 degree incidence), and a set of manifolded 'Static' tapping on the cylindrical body. The design is based on one found in [14]. Calibration data for these were collected in a separate wind tunnel experiment and were found to be independant of speed over the range expected on the turbine. The angle of attack calibration is very linear over a range of +/- 15 degrees and still smooth up to +/- 30 degrees, a

function based on angle of attack and the pressure readings from all six ports is calculated to represent the calibration.

- The positions of the tappings and probes were chosen based on modelling with a blade element model providing the angle of attack input to a two dimensional panel code. The resulting positioning for the surface tappings is typical of aerofoil experiments, however the position of the probes is perhaps novel, not being straight out from the leading edge. The panel code was used to indicate a velocity field around the section, and iterated through the likely range of angle of attack, then for each point the variance of direction compared with the incident flow was calculated. A region emanating from roughly a third of a chord behind the leading edge and in a direction about 45 degrees from the chord line on the pressure side had a region of minima, so the probe head is placed in this region oriented to aim at the mean inflow direction.

Tubing, pressure transducers and measuring speed

The surface pressure tappings and probe ports are connected by tubes (diameter 1mm, up to 1.3 m long) to 64 port differential Scannivalve pressure transducer blocks, each block serving two stations and one probe. These have 32 sensors each, a valving system (pneumatically operated) switches the sensors to look at two sets, thus covering the 64 inputs. Ths scanning between sensors is achieved (electronically) by multiplexing the input to the block's amplifier. The transducer blocks can operate at 20,000 samples per second, thus a scan of all 32 sensors will take just under 2 milliseconds. The blocks are enclosed in thermally controlled and insulated boxes to keep their temperature above condensation temperature and to maintain accuracy of the sensors.

Other measurements from the rotor

- Azimuth position: An incremental shaft encoder which gives 2880 pulses per revolution provides positional information and is used for the triggering of data scans.
- Root bending moments: Two strain gauge bridges for flatwise and edgewise moments have been included which can help to confirm summed blade forces.
- Temperatures: The pressure sensors' main source of error is due to drift from temperature effects, so as well as the thermal control, the temperature of the blocks are measured by platinum resistance thermometers (PRT). A separate PRT is mounted on the inner surface of the blade skin to give local temperature.
- Reference Pressure: This is included for on-line calibration of the main pressure transducers. It has very good linearity (< 0.01 % FSD) and repeatability.

Interfacing, Control and Signal Conditioning

The transducers require significant control, both electronic and pneumatic, this is needed for multiplexing and routing of reference and calibration pressures. This system includes custom digital electronics controlled by the loggin PC. The signal conditioning for the PRT's and strain gauges is included in this unit.

Software

This software is written in 'Turbo Pascal' with some assembler code subroutines for speed. The 'Turbo Pascal' development environment is installed on the hub logging computer to aid debugging, it is useful because it is very compact.

The data collection regimes and supervisory actions are controlled by first editing a 'Recipe' file, sending it to the hub-logger and then running the data collection

program based on these settings.

Communication link
The hub logger communicates, through Fibre Optic link to another PC, in the test site control building about 150 m away. A Fibre Optic link was chosen to be sure of no problems with range and to provide immunity for the site's quite high electromagnetic interferences.

Ground fixed measurements
The ground PC is in the same building as an existing logging system (from wind diesel research). During these experiments a pulse is sent from the hub synchronised with scans of the pressure sensors to trigger this logger - it measures:
- Electrical machine power from fast response (40 ms) power transducers.
- Yaw position from an analogue shaft encoder.
- Incident wind speed and direction from two meteorology masts, two diameters away from the turbine, the instruments are at hub height (15.5 m).
- Ambient air pressures and temperatures

4.2.3 Data reduction

- The MATLAB environment has been used to handle most of the data processing, thus the first process is to load the raw data files from the two logging systems
- There have been some problems with data corruption - some of the error were correctable coding errors and have been fixed, others have been corrected using multipoint median filters.
- The data has been calibrated to engineering units and the synchronisation (between the two streams) has been checked. The result has then been stored in the MATLAB format (IEEE double precision floating point) as the working set. No filtering has been carried out on this data.
- From the pressure data, the blade geometry and wind tunnel probe calibrations the following have been derived: o Section lift forces per unit length o Inflow direction and dynamic pressures at the probes These do not include corrections for centrifugal effects, thus the pressures are effectively as if they were measured at the sensor radius, which is approximately the same as the probe radius.

Notes:
- Lift forces are calculated using the fractional chord length positions of the tapping holes thus are: per unit span, per unit chord; thus all that remains to determine the coefficients is to divide by an appropriate dynamic pressure.
- The inflow measurement include the outwash angle (compared with the tangent) thus direction and velocity CAN be corrected according to the geometry of the blade.
- Inflow and lift coefficients have been obtained as follows:
  - The air density is assumed constant over the site thus the site meteorology measurements are used to obtain an air density, thus the velocity at the probe can be determined. This is transferred to test section radius by adding (or subtracting) the difference in radial velocities. The dynamic pressure is then recalculated as two components. The angles are corrected assuming that the probe remains at the same proportional relative position compared with the chords at its radius and at the test radius. The Angle of Attack (at transferred

probe position) is then:

$$\alpha_{Pr} = \arctan(\frac{V_{ax}}{V_{tan}}) - \theta \tag{4.1}$$

with V_{ax} the axial speed and V_{tan} the tangential speed and the dynamic pressures are:

$$q_{Pr,a} = 1/2 \cdot \rho \cdot (V_{ax}^2 + V_{tan}^2) \tag{4.2}$$

$$q_{Pr,b} = 1/2 \cdot \rho \cdot (V_{outwash}^2) \tag{4.3}$$

with $V_{outwash}$ the outwash speed.

– Using the above angle and the angle of the section lift force:

$$\alpha_L = \arctan(\frac{t}{n}) \tag{4.4}$$

a quadratic relation is fitted for low angles and extrapolated to larger angles. This assumes that the pressure distribution represents the components of lift found in inviscid theory (which always has its lift force perpendicular to the flow).

– The dynamic pressure measured at the probe ($q_{Pr,a}$, above) has been used as the denominator for calculation of the coefficients. This is known not to be accurate as upwash also affects this - a similar process to the angle of attack correction is needed.
A study with a reliable 2-D Navier-Stokes solver may be interesting to support or correct this method - the components of force caused by skin friction must be treated separately in the analysis - standard aerofoil packages automatically sum them before presentation to the user.

Figure 4.12 *Instrumentation of probes at IC/RAL blade*

4.3 NREL test turbine

The aerodynamic experiments at NREL were performed in four different phases, see below. Measurements from the phases II, III and IV are stored into the database.

4.3.1 Global characteristics of facility

- Blade: NREL in house, mounted on an experimental turbine.
- Number of blades: 3
- Blade span (from flange to tip) = 4.521 m
- Rotor diameter = 10 m
- Blade profile: NREL S809
- Two tests:
  - Phase II: Blade without twist and taper
  - Phase III and IV: Blade without taper but with twist: Twist = 45 degrees.
- Detailed pressure tap measurements around profiles at 4 (Phase II) or 5 (Phase III and IV) different radial stations. Pairs of taps at 6 (Phase II) or 10 (Phase III and IV) different radial stations.
- Inflow angle is measured at the 4 or 5 primary stations with wind vanes (Phase II and Phase III) or 5-hole probes (Phase IV). Inflow velocity is measured at the 4 or 5 primary stations with pitot probes (Phase II and Phase III) or 5-hole probes (Phase IV).

Location

All atmospheric testing was conducted at the National Renewable Energy Laboratory's (NREL) National Wind Technology Center (NWTC) located 10 miles north of Golden, Colorado, U.S.A. Winter winds are dominant at this site from a prevailing direction of 292 degrees from True North. Although the local terrain is flat, with grassy vegetation extending over 0.8 km upwind, the site is situated approximately 5 km from the base of the Rocky Mountains which are located directly upwind. The wind turbine was unobstructed by other wind turbines or structures.

Experiment overview

The Combined Experiment was begun in 1987 and continues today under the title of the Unsteady Aerodynamics Experiment. The program was divided into four phases. Phase I planning began in 1987 and resulted in valuable knowledge and experience with these types of measurements (Butterfield et al., [15]). Untwisted blades were used again in Phase II which began in the spring of 1989, and the pressure instrumentation was expanded to four span locations. Optimally twisted blades were designed for Phase III of the project which began in 1993. The fourth phase, initiated late 1995, also used the twisted blades but the flow angle measurements were improved. The significant differences between the Phase II, Phase III, and Phase IV configurations are described in table 4.1 below.

Test Turbine

The Unsteady Aerodynamics Experiment Test Turbine is a modified Grumman Wind Stream 33. It is a 10-m-diameter, three-bladed, downwind, free-yaw turbine equipped with full span pitch capability that can be manually controlled during the testing to provide fixed-pitch (stall-controlled) operation at any pitch angle desired. The turbine is supported on a guyed-pole tower, 0.4064 m in diameter,

Table 4.1 *Unsteady Aerodynamics Experiment Configuration Differences*

	Phase II	Phase III	Phase IV
Blades	Untwisted	Twisted	Twisted
Local Flow Angle (LFA) Measurement Device	Flag	Flag	5-Hole Probe
Span locations instrumented with LFA sensors	4	4	5
Span locations instrumented with pressure taps	4	5	5
Azimuth angle measurements and RPM calculations	Poor	Good	Good
Meteorological instrumentation	Vertical Plane Array	Horizontal and Vertical Shear	Horizontal and Vertical Shear
Selections of data during which yaw brake engaged	Yes	No	Yes
Campaign Duration	5 minutes	10 minutes	10 minutes
Boom extension and camera mounted on hub	Yes	No	Yes
Video	Yes	No	Yes

that is equipped with a hinged base and gin pole to allow it to be tilted down easily. An electric winch is used to lower and raise the system during installation. A manually operated yaw brake was added to allow fixed yaw operation at arbitrary yaw positions. This yaw retention system had a strain-gaged link to measure yaw moments in Phase II and Phase IV. A relatively constant yaw angle and non-zero yaw moment indicates the yaw brake was engaged during data acquisition. Also added was a mechanical caliper rotor brake system that could be operated manually from the control shed. A complete listing of turbine specifications may be found in Appendix E.

The drive train is unchanged from the original Grumman configuration. The rotor operates at a nominal 72 rpm. Low-speed shaft torque is transferred through a 25.1:1 gearbox ratio to the high-speed shaft which is connected to the generator. The inertia of the Phase IV rotor (twisted blades, instrumentation boxes, boom, hub, and camera) was determined by measuring low-speed shaft torque, power, and rpm during turbine start-up. An estimate of drive train (low-speed shaft, gearbox, and high-speed shaft) stiffness was also obtained from this test. The inertia of the entire rotating system (rotor and drive train) was measured with a pendulum test. Data collected during operation of the instrumented turbine provided measurements of the generator slip and total efficiency of the drive train. The machine description in Appendix E lists all of these results, and the layout of the nacelle is pictured in figure 4.13.

The most significant configuration change to the original Grumman turbine was the blade design. The NREL S809 airfoil replaced the original Grumman airfoil. The S809 airfoil was developed by Airfoils, Inc., under contract to NREL (Somers, Unpublished, [16]). The primary reason this airfoil was chosen was that a well-documented wind tunnel data base that included pressure distributions, separation boundary locations, drag data, and flow-visualization data was available. The S809 airfoil was used in both the untwisted and twisted configurations which are pictured in Figures 4.14 and 4.15, respectively.

Figure 4.13 *NREL: Nacelle layout*

The untwisted and twisted blades were similar in design and fabrication. Both had a constant 0.457 m chord, and a planform view of the blades is shown in Figure 4.16. The intent in the design of twisted blades was to maintain a constant angle of attack along the span of the blade at a wind speed of 8 m/s (Simms, Fingersh, and Butterfield, [17]). The twist distribution of the blades used in Phases III and IV is listed in Appendix E. The thickness and airfoil distribution of the twisted blades were nearly identical to that of the untwisted blades with the spar enlargement extending to 25% span instead of 30% span. Both sets of blades were fiberglass/epoxy composite, but the spar in the twisted blades was carbon fiber as opposed to the fiberglass/epoxy spar used in the untwisted blades. They were designed to be stiff to mitigate aeroelastic blade responses. The dynamic characteristics of the blades were tailored to avoid coalescence of rotor harmonics with flap-wise, edge-wise, and torsional natural frequencies. To minimize the possibility of aeroelastic instabilities, the mass and elastic axes were aligned with the aerodynamic axis. The instrumented blade was painted black to contrast with the white tufts that were used for flow visualization. The pitch shaft is less stiff than the inboard sections of the blade, and most of the flap deflection occurs in this region. For this reason, the pitch shaft must be included in a blade or hub model and is included with the estimated blade mass and stiffness distributions in Appendix E.

Meteorological (Met) Towers

During Phase II, the inflow conditions were measured at three locations in the predominantly upwind direction (292 degrees): the North met tower, the Local met tower, and the Vertical Plane Array (VPA). The North met tower was 50 m tall and located 500 m upwind of the turbine. Large-scale atmospheric inflow conditions were measured at this location in the form of wind speed and direction at four elevations (5 m, 10 m, 20 m, and 50 m), temperature at 5 m and at 50 m, and barometric pressure. Local inflow measurements were made 12 m upwind

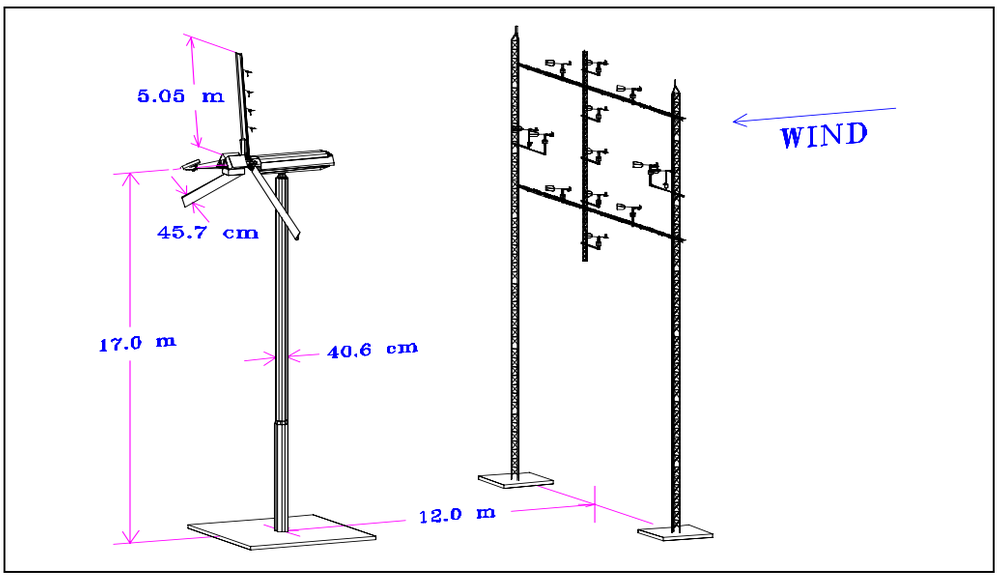

Figure 4.14 *NREL: Phase II (untwisted blade) test configuration*

of the turbine on the VPA which is depicted in figure 4.17. Two Rohn 45-G guyed met towers supported three cross-booms, where 11 prop-vane and 2 bi-vane anemometers measured inlet flow magnitude and direction. Eight of the prop-vane anemometers were arranged in a circle corresponding to 80% of the blade span at approximately hub height. The remaining prop-vane anemometers were spaced evenly inside the circle. The two bi-vane anemometers were mounted outside the circle on the horizontal axis. Also located 12 m upwind of the turbine and 20 m to the north was the 16.8 m Local met tower. Sonic anemometer measurements and hot-film temperature measurements originated from this tower, but this data was not available for selections placed in the data base. Detailed discussion of the anemometry used in the Phase II portion of the experiment appears in Butterfield et al., ([15]). Table 4.2 lists all of the channels related to measurements made on the Phase II met towers that were included in the data base.

In order to comply with the conventions established by the Annex, all of the wind direction measurements were converted to yaw error measurements by subtracting the turbine angle. These angles were measured in accordance with the counter-clockwise rotating turbine convention.

Inflow conditions were again measured directly upwind of the turbine during Phases III and IV, but the North met tower was not used. Instead, a taller Local met tower was used to measure shear and stability near the turbine. Three met towers placed 1.5D upwind of the turbine supported multiple cup anemometers, bi-vane anemometers and one sonic anemometer. The cup anemometers provided more accurate wind speed measurements than the prop-vane anemometers used during Phase II because the cup anemometers have a higher frequency response and are not susceptible to gyroscopic effects. Temperature and barometric pressure

Table 4.2 *Phase II (Untwisted Blade) Local Inflow Measurements*

Identification	Description	Units
V(w,1)	VPA Prop Vane Wind Speed (6:00)	m/s
V(w,2)	VPA Prop Vane Wind Speed (6:00 @ 40% Span)	m/s
V(w,3)	VPA Prop Vane Wind Speed (4:30)	m/s
V(w,4)	VPA Prop Vane Wind Speed (7:30)	m/s
V(w,5)	VPA Bi-Vane Wind Speed (3:00 @ 100% Span)	m/s
V(w,6)	VPA Prop Vane Wind Speed (3:00)	m/s
V(w,7)	VPA Prop Vane Wind Speed Hub Height	m/s
V(w,8)	VPA Prop Vane Wind Speed (9:00)	m/s
V(w,9)	VPA Bi-Vane Wind Speed (9:00 @ 100% Span)	m/s
V(w,10)	VPA Prop Vane Wind Speed (1:30)	m/s
V(w,11)	VPA Prop Vane Wind Speed (10:30)	m/s
V(w,12)	VPA Prop Vane Wind Speed (12:00 @ 40% Span)	m/s
V(w,13)	VPA Prop Vane Wind Speed (12:00)	m/s
V(w,14)	North met Wind Speed 5m	m/s
V(w,15)	North met Wind Speed 20m	m/s
V(w,16)	North met Wind Speed 50m	m/s
phi(y,1)	VPA Bi-Vane Wind Direction (3:00 @100% Span) - Yaw Angle	deg
phi(y,2)	VPA Bi-Vane Wind Direction Hub Height - Yaw Angle	deg
phi(y,3)	VPA Bi-Vane Wind Direction (9:00 @100% Span) - Yaw Angle	deg
phi(y,4)	North met Wind Direction 5m - Yaw Angle	deg ')
phi(y,5)	North met Wind Direction 10m - Yaw Angle	deg ')
phi(y,6)	North met Wind Direction 20m - Yaw Angle	deg
phi(y,7)	North met Wind Direction 50m - Yaw Angle	deg
alpha (w,1)	VPA Bi-Vane Wind Elevation Angle (3:00 @100% Span)	deg
alpha (w,2)	VPA Bi-Vane Wind Elevation Angle (9:00 @100% Span)	deg
5mairT	North met Temperature 5m	K
deltaT	North met Delta Temperature (50m-5m)	K
Baro Press	Barometric Pressure	Pa

') These channels do not appear in all data base selections.

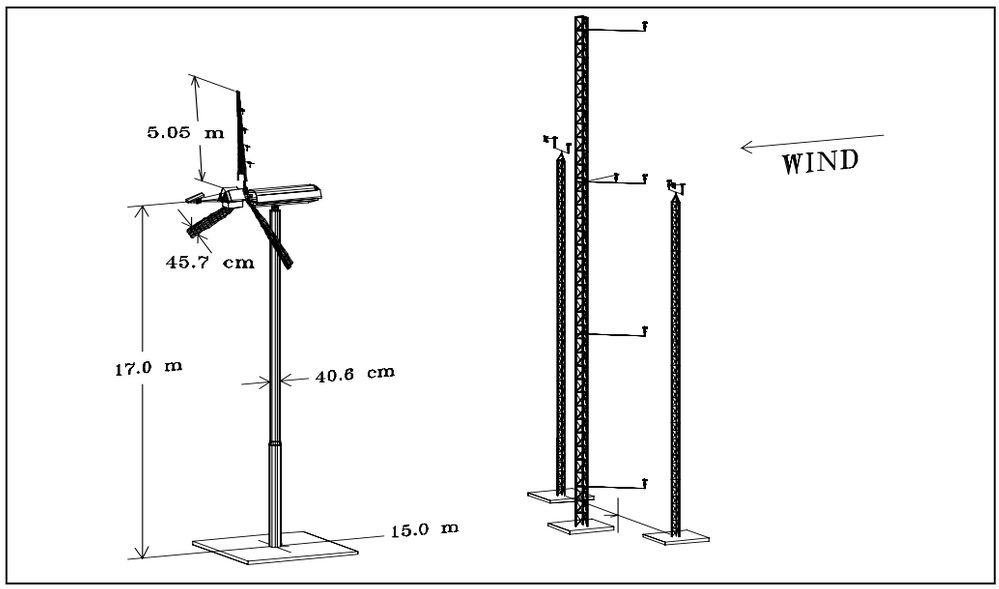

Figure 4.15 *NREL: Phase III and Phase IV (twisted blade) test configuration*

measurements were also made. Figure 4.18 shows the three instrumented met towers. Phase III and Phase IV meteorological channel descriptions are shown in table 4.3.

4.3.2 Instrumentation

Pressure taps

The most important yet most difficult measurements were the blade surface pressures. The quality of the aerodynamic performance coefficients depends on the accuracy of individual pressure tap measurements. Each coefficient for a particular radial station was the integrated value of the measured pressure distribution. The measurement approach was to install small pressure taps in the surface of the blade skin. Each opening was mounted flush to the airfoil surface and was 1.016 mm in diameter. The flush profile was necessary to prevent the taps themselves from disturbing the flow. Stainless steel tubes, 0.15 m in length, were installed inside the blade's skin during manufacturing to carry surface pressures to the pressure transducer. A short piece of plastic tubing joined the tubes to the transducers. The taps were aligned along the chord (instead of being staggered) so that spanwise variations in pressure distributions would not distort measured chord-wise distributions. As illustrated in Figure 4.19, the taps were concentrated toward the leading edge to achieve stronger resolution in the more active areas of the pressure distributions.

The Phase II experiment used 28 pressure taps at four primary radial locations: 30% span, 47% span, 63% span, and 80% span. During Phases III and IV, 22 taps were instrumented at five primary spanwise locations: 30% span, 47% span,

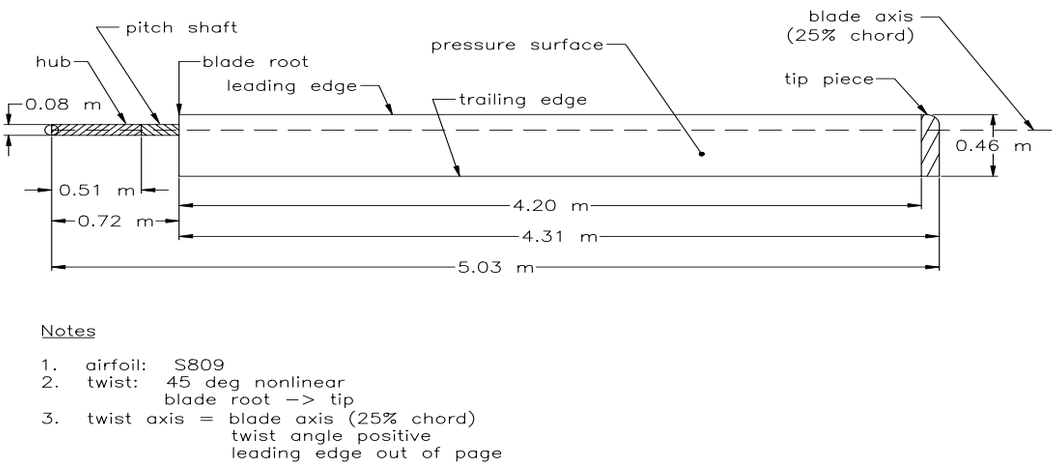

Figure 4.16 *NREL: Planform of the blades*

63% span, 80% span, and 95% span. Pairs of taps at 4% chord and 36% chord were installed at various other intermediate span locations (36%, 41%, 52%, 58%, 69%, 74%, 85%, 90%, 92%, and 98%). Figure 4.19 depicts the blade layout for Phase III. Recall that there were no pressure taps outboard of 80% span during Phase II.

Based on tests performed in the first phase of the experiment, dynamic corrections were deemed unnecessary (Butterfield et al., [15]). Gain amplifications and phase effects that occur as a function of tube frequency and tube length were measured. These effects were not significant up to a frequency of 80 Hz, and the measured pressure data showed no appreciable information above 40 Hz.

Pressure Transducer

Because the dynamic pressure varied significantly along the span due to rotational effects, transducers with different measurement ranges were used. The nominal transducer ranges used during different test phases are listed in table 4.4. The transducers, Pressure Systems model ESP-32, scanned port to port at 16,667 Hz completing a scan of all pressure taps at approximately 520 Hz. One transducer was used at each primary span location to measure up to 32 channels of differential pressures between the pressure taps (local static pressure) and the reference pressure located in an instrumentation box mounted on the hub. Each transducer was installed inside the blade as close to the pressure taps as possible. These electronic scanner-type transducers provided remote calibration capability through a pneumatically operated valve. The capacity to purge all of the pressure taps with dry nitrogen was used periodically to prevent moisture or small particles from affecting the pressure measurements.

Table 4.3 *Phase III and Phase IV (Twisted Blade) Local Inflow Measurements*

Identification	Description	Units
V(w,1)	Local met Wind Speed 2.4m	m/s
V(w,2)	Local met Wind Speed 10.06 m	m/s
V(w,3)	North local met Wind Speed 17.02m (hub height)	m/s
V(w,4)	Local met Wind Speed 17.02m (hub height)	m/s
V(w,5)	Sonic nr. 1 Wind Speed (horizontal) 17.02m (hub height)	m/s
V(w,6)	South local met Wind Speed 17.02m (hub height)	m/s
V(w,7)	Local met Wind Speed 24.38m	m/s
phi(y,1)	North local met Wind Direction 17.02m (hub height) - yaw angle	deg
phi(y,2)	Sonic nr. 1 Wind Direction 17.02m (hub height) - yaw angle	deg
phi(y,3)	South local met Wind Direction 17.02m (hub height) - yaw angle	deg
alpha(w,1)	North local met Wind Elevation Angle 17.02m (hub height)	deg
alpha(w,2)	South local met Wind Elevation Angle 17.02m (hub height)	deg
2mairT	Local met temperature 2.4m	K
24mairT	Local met temperature 24.48m	K ')
22mdT	Local met delta temperature (24m-2m)	K ')
2mdpT	Local met dewpoint temperature 2.4m	K
Baro Press	Barometric pressure	Pa

') These channels do not appear in all data base selections.

Table 4.4 *Nominal, Full-Scale, Pressure Transducer Measurement Ranges*

	Phase II	Phase III and Phase IV
30% Span	+/- 2970 Pa (0.4 psi)	+/- 2488 Pa (10" H2O)
47% Span	+/- 2970 Pa (0.4 psi)	+/- 2488 Pa (10" H2O)
63% Span	+/- 8274 Pa (1.2 psi)	+/- 4977 Pa (20" H2O)
80% Span	+/- 8274 Pa (1.2 psi)	+/- 10, 342 Pa (1.5 psi)
95% Span		+/- 10, 342 Pa (1.5 psi)

Figure 4.17 *NREL: Phase II (Untwisted blade) Meteorological instrumentation; Side view looking downwind toward 292 degrees. Meteorological instruments are 1.2D (12 m) upwind of the turbine tower.*

Pressure System Controller (PSC)

Remote control of ESP-32 pressure transducer calibration, scanner addressing, and demultiplexing of the analog multiplexed signals were performed by the PSC, a hub-mounted microprocessor control unit designed by NREL (Butterfield et al., [15]). The PSC was completely redesigned from Phase II to Phase III to improve the accuracy and the user interface. Currently up to 155 pressure channels may be processed simultaneously. All pressure ports were scanned at 520 Hz with a port-to-port settling time of 60 microsec. The objective was to provide 100 Hz bandwidth frequency response to enable study of dynamic stall behavior on the rotating wind turbine blade.

Once the PSC scanned the pressure port addresses, the samples were passed as digital signals to the pulse code modulation (PCM) encoder. The PCM system

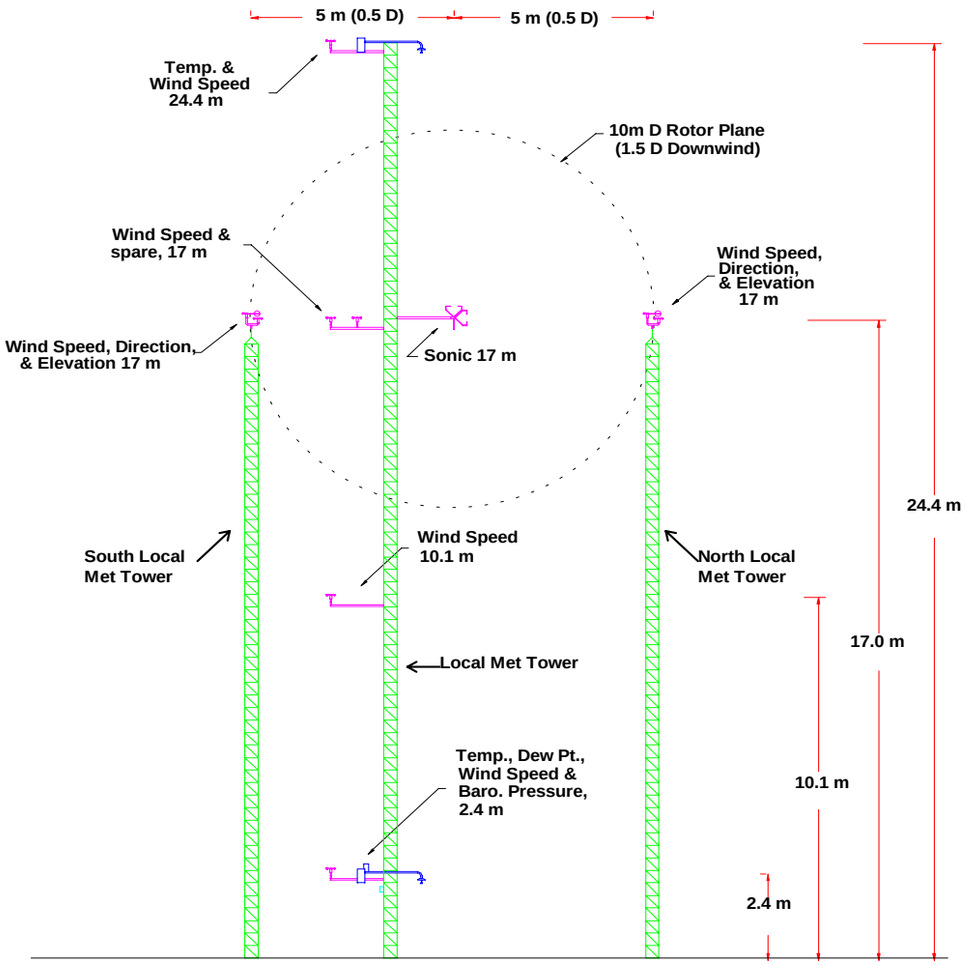

Figure 4.18 *NREL: Phase III and Phase IV (twisted blade) Meteorological instrumentation; Side view looking downwind toward 112 degrees. Meteorological instruments are 1.5D (15 m) upwind of the turbine tower.*

multiplexed the 62 channels of data into one data stream which was conducted through a single coaxial cable. The PCM streams were passed over slip rings to the control building and were recorded on optical disk for later processing.

The PSC pneumatic control valves and ramp calibration sequence is discussed in the Phase I report ([15]) and summarized in section 4.3.3. The only changes between Phase II and Phases III and IV were that a more accurate calibration reference pressure was used, and calibrations were automated by a computer-controlled processing system.

Local Flow Angle (LFA) Transducers

Geometric angle of attack (AOA) measurements are fairly easy to make in a wind tunnel where the air flow is precisely controlled, but in the field environment the

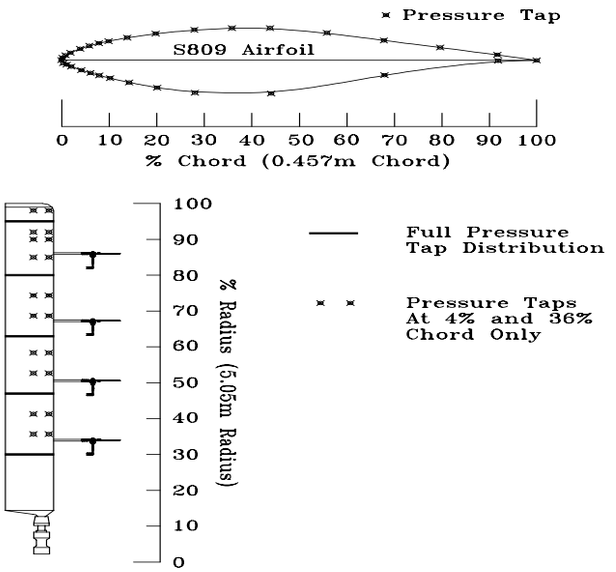

Figure 4.19 *NREL: Configuration of Phase III (twisted) instrumented blade. During Phase II, there were no taps outboard of 80% span. During Phase IV, the local flow angle flags were replaced with 5-hole probes at all 5 primary locations*

difficulty in obtaining angle of attack measurements increases. To accomplish this, it was necessary to make measurements of the local inflow in front of the blade. The flow angle sensor illustrated in Figure 4.20 was developed by NREL for this purpose (Butterfield et al., [15]) and was used in Phase II and Phase III tests. It consisted of a lightweight, rigid flag that aligned itself with the local flow. During Phase II tests, a commercial rotary position sensor mounted in a custom housing measured the flag angle within 1.0 degree accuracy over the range of -20 deg to 40 deg The analog signals generated were sent to the hub, multiplexed, and recorded with the other signals by the data acquisition system. This analog position encoder was replaced with a digital resolver during Phase III testing. The flag extended 36 cm (34 cm during Phase II) ahead of the leading edge and was aligned with the pressure taps. The sensor was attached to the blade 4% outboard of the four primary pressure stations (30%, 47%, 63%, and 80%) in order to minimize flow disturbances on the blade near the pressure taps. During Phase II the flag sensor was actually mounted at 86% span measuring a local flow angle at 82% span instead of 80% span. However, in the data base files corresponding to the Phase II test, this local flow angle is associated with the 80% span pressure tap location. Processing of the data revealed that during Phase II the flag at 47% span did not work properly for most of the duration of testing so it was removed from the processed data files. Table 4.5 describes the local flow angle measurements for Phase II and Phase III.

During Phase III, a five-hole probe was mounted 4% inboard of the 95% span

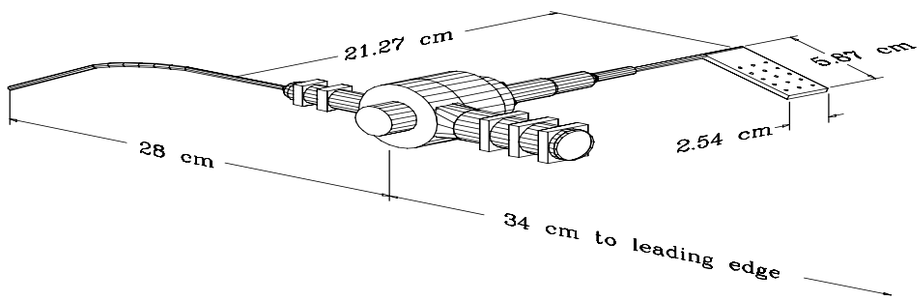

Figure 4.20 *NREL: Phase II Flag Local Flow Angle sensor. During Phase III, the sensor was located 36 cm from the leading edge*

Table 4.5 *Phase II and Phase III Local Flow Angle Measurements (Flag)*

Identification	Description	Units
alpha (m,1)	30% Local Flow Angle (LFA) (Flag)	deg
alpha(m,4)	47% Local Flow Angle (LFA) (Flag)	deg ')
alpha(m,7)	63% Local Flow Angle (LFA) (Flag)	deg
alpha(m,10)	80% Local Flow Angle (LFA) (Flag)	deg '')

') Phase III only

'') actually measured at 82% span during Phase II

pressure station in order to test this new device for measuring local flow angle. This data was not included in any of the Phase III files supplied to the Annex XIV data base, but the test did prove that the five hole probe provided greater dynamic response than the flag which is necessary in studying dynamic stall (Fingersh and Robinson, [18]). Therefore all of the flag sensors were replaced with five hole probes during Phase IV testing. The probes, depicted in Figure 4.21, extended 37 cm ahead of the leading edge at an angle 20 degrees below the chordline and measured local flow angles over the range -15 to 55 degrees. Each probe was mounted 4% span outboard of the primary pressure stations except at the 95% pressure tap station where the probe was mounted 4% span inboard. Note that the local flow angle measurement from the probe is no longer aligned with the full-chord pressure measurements as was the local flow angle measured with the flag. These measurements were identified with the corresponding percent span location instead of the corresponding pressure station number as were the flag measurements. In addition to the local flow angle, the five hole probes used in Phase IV provided measurement of the dynamic pressure and spanwise flow angle. Neural network models were used to create a surface based on data obtained from wind tunnel probe calibrations (Fingersh and Robinson, [18]). Resulting surfaces were implemented as lookup tables in the post-processing software. The pressures

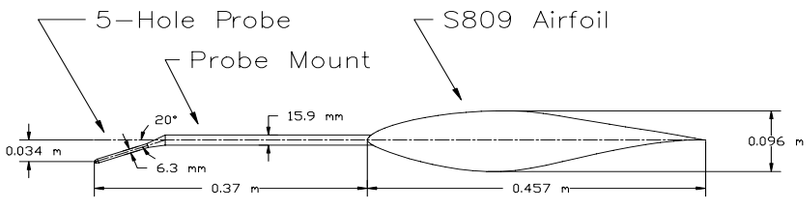

Figure 4.21 *NREL: Phase IV Five hole-probe local flow sensor.*

Table 4.6 *Phase IV Local Flow Angle Measurements (5-Hole Probe)*

Identification	Description	Units
alpha(m,34)	34% Local Flow Angle (LFA) (5-hole probe)	deg
alpha(m,51)	51% Local Flow Angle (LFA) (5-hole probe)	deg
alpha(m,67)	67% Local Flow Angle (LFA) (5-hole probe)	deg
alpha(m,84)	84% Local Flow Angle (LFA) (5-hole probe)	deg
alpha(m,91)	91% Local Flow Angle (LFA) (5-hole probe)	deg
alpha(x,34)	Crosswise flow angle at 34% span	deg
alpha(x,51)	Crosswise flow angle at 51% span	deg
alpha(x,67)	Crosswise flow angle at 67% span	deg
alpha(x,84)	Crosswise flow angle at 84% span	deg
alpha(x,91)	Crosswise flow angle at 91% span	deg

from each of the five holes in the probe were recorded, but only the resulting dynamic pressure, local flow angle, and crossflow angle were included in the data base. Table 4.6 describes the local flow angle measurements made during Phase IV.

Strain Gages and Accelerometers

Blade, tower, rotor, and yaw loads were measured with strain gages during Phase II testing. Five spanwise locations on the instrumented blade, root (8% span), 20% span, 40% span, 50% span, and 90% span, were instrumented with strain gages to measure blade flap-wise bending while two locations, root (8% span) and 50% span, were instrumented to measure edge bending. Blade pitching moment (blade torsion) was measured at the root (8% span), 50% span and 70% span. Root flap and edge bending moments were also measured on the other two blades. Bending of the low speed shaft in two orthogonal planes was measured as well as the low speed shaft torque. Loads in the non-rotating environment were also measured. Gages were mounted on two tower bending axes at the point just above

Table 4.7 *Phase II (Untwisted Blades) Load Measurements*

Identification	Description	Units
M(1)	Strain Blade 1A, root flap bending moment	Nm
M(2)	Strain Blade 1B, root flap bending moment	Nm
M(3)	Strain Blade 1, root edge bending moment	Nm
M(4)	Strain Blade 1, 20% flap bending moment	Nm
M(5)	Strain Blade 1, 40% flap bending moment	Nm
M(6)	Strain Blade 1, 50% flap bending moment	Nm
M(7)	Strain Blade 1, 50% edge bending moment	Nm
M(8)	Blade 1 torsion at 50% span	Nm
M(9)	Blade 1 torsion at 70% span	Nm ')
M(10)	Strain Blade 1, 90% flap bending moment	Nm
M(11)	Strain Blade 2, root flap bending moment	Nm
M(12)	Strain Blade 3, root flap bending moment	Nm
M(13)	Strain X-X Low speed shaft bending moment (horizontal axis)	Nm
M(14)	Strain Y-Y Low speed shaft bending moment (vertical axis)	Nm
M(15)	Strain Low speed shaft torque A	Nm
M(16)	Strain Low speed shaft torque B	Nm
M(17)	Blade 1 root torque (link)	Nm
M(18)	Tower bending moment about East-West Axis (X)	Nm
M(19)	Tower bending moment about North-South Axis (Y)	Nm
M(20)	Yaw Moment	Nm
M(21)	Estimated Aerodynamic Thrust	N
M(22)	Estimated Aerodynamic Torque	Nm

') These channels do not appear in all data base selections.

the guy wire attachment. These gages were oriented to measure bending parallel and perpendicular to the direction of the prevailing wind. Gages were mounted on the arm of the yaw brake to measure yaw moment when the yaw brake was engaged. All load measurements corresponding to Phase II tests are listed in table 4.7. Estimates of aerodynamic thrust and torque resulting from methods described in section 4.3.3 were also included in the data base.

Similar measurements were made during Phases III and IV testing periods. Flap and edge bending moments were recorded from strain gages mounted at the root (8% span), 25%, and 60% span on the instrumented blade. Flap and edge bending measurements were taken at the root of the other two blades, and low speed shaft bending in two planes as well as low speed shaft torque measurements were also obtained. There were no pitching moment measurements made in either of these phases of the experiment. Instead of measuring tower bending with strain gages, accelerometers were placed in the nacelle to determine yaw, pitch and fore-aft motion. Accelerometers in the tip of each blade measured movement in the flap and edge directions. During Phase IV, strain gages were used to measure yaw moment. These measurements are listed in table 4.8 below.

Strain gages measuring root flap and edge loads were applied to the steel pitch shaft adjacent to the blade attachment location. The pitch shaft was reduced to a uniform, cylindrical, 80 mm diameter at 8% span, the location where the strain gages were applied. The uniform, cylindrical region eliminates geometry effects

Table 4.8 *Phase III and Phase IV (Twisted Blade) Load Measurements*

Identification	Description	Units	comment
M(1)	Strain Blade 1 root flap bending moment	Nm	
M(2)	Strain Blade 1 root edge bending moment	Nm	
M(3)	Strain Blade 1 25% flap bending moment	Nm ')	
M(4)	Strain Blade 1 25% edge bending moment	Nm ')	
M(5)	Strain Blade 1 60% flap bending moment	Nm ')	
M(6)	Strain Blade 1 60% edge bending moment	Nm ')	
M(7)	Accelerometer Blade 1-Flap	m/s^2	
M(8)	Accelerometer Blade 1-Edge	m/s^2	
M(9)	Strain Blade 2 root flap bending moment	Nm	
M(10)	Strain Blade 2 root edge bending moment	Nm	
M(11)	Accelerometer Blade 2-Flap	m/s^2	
M(12)	Accelerometer Blade 2-Edge	m/s^2	
M(13)	Strain Blade 3 root flap bending moment	Nm	
M(14)	Strain Blade 3 root edge bending moment	Nm	
M(15)	Accelerometer Blade 3-Flap	m/s^2	
M(16)	Accelerometer Blade 3-Edge	m/s^2	
M(17)	Strain X-X Low speed shaft bending moment	Nm	
M(18)	Strain Y-Y Low speed shaft bending moment	Nm	
M(19)	Strain Low speed shaft torque	Nm	
M(20)	Nacelle Accelerometer Yaw	m/s^2	
M(21)	Nacelle Accelerometer Fore-Aft	m/s^2 ')	
M(22)	Nacelle Accelerometer Pitch	m/s^2	
M(23)	Estimated Aerodynamic Thrust	N	Phase III
M(24)	Estimated Aerodynamic Torque	Nm	Phase III
M(23)	Nacelle Yaw Moment	Nm	Phase IV
M(24)	Estimated Aerodynamic Thrust	N	Phase IV
M(25)	Estimated Aerodynamic Torque	Nm	Phase IV

') These channels do not appear in all data base selections.

while measuring flap and edge bending moments. This cylindrical section of the blade root is illustrated in figure 4.19.

Strain gages on the instrumented blades consisted of four active gage elements mounted inside the fiberglass blade skin. The gages were installed inside the skin during the blade manufacturing process to preserve the exterior airfoil shape and surface smoothness. The strain gages were positioned carefully to minimize flap-wise and edge-wise cross-talk. A maximum of 4% cross-talk was measured during the blade pull and strain gage calibration tests (Butterfield et al., [15]). These cross-channel interference effects were not considered significant, and corrections were not applied to the data.

Calibration of the low-speed shaft torque channel introduced errors during phase II and phase III. Equations that correct for the calibration errors are included in Appendix Appendix E.

Miscellaneous Transducers

Various sensors were used to measure yaw position, pitch angle and rotor azimuth position. In Phase II, gear-driven potentiometers were used to measure yaw position and pitch angle of the instrumented blade. The rotor azimuth position was measured with an analog rotary position encoder connected to the low-speed shaft via a gear and chain. This device created discontinuities and non-linearities due to its physical limitations in the transition from 0 to 360 degrees. The data were therefore corrected during post-processing through insertion of an idealized saw-tooth between adjacent 180 degree transition points. This provided a clean transition from 0 to 360 degrees and smooth linear values throughout the rest of the cycle. However, the rotational frequency channel (RPM), calculated during post-processing, was affected by this smoothing of the data so it must be regarded with speculation.

During Phases III and IV, gear-driven, BEI model R-25 optical absolute position encoders replaced the gear-driven potentiometers measuring yaw position and rotor azimuth position. Each of the blades was instrumented with an encoder for pitch measurements. These digital measurements significantly reduced uncertainty in subsequent measurements.

Generator power was monitored using an Ohio Semitronics, Inc. (OSI) power watt transducer during all phases of testing. Absolute reference pressure was measured using a Setra 270 Absolute Pressure transducer located inside the instrumentation box containing the reference pressure during Phase II only. All of these miscellaneous channels are listed in table 4.9.

Flow Visualization

Flow visualization was achieved through the use of tufts attached to the surface of the blade during Phase II and Phase IV testing. The tufts were made of thin, white, polyester thread measuring approximately 0.25 mm in diameter and 45 mm in length. A small drop of fast drying glue held each of the tufts to the downwind side of the instrumented blade. Tufts were placed in rows spaced 76 mm apart in the blade spanwise direction.

Two high-shutter-speed cameras were mounted in the rotating frame during Phase II and Phase IV testing. A Panasonic camera with a Rainbow zoom lens and remote control iris and focus adjustments was mounted on the end of a lightweight, 3 m boom which was attached to the hub, as shown in figure 4.15. The boom was

Table 4.9 *Phase II, Phase III, and Phase IV Miscellaneous Transducers*

Identification	Description	Units
phi(r,b)	Blade azimuth angle	deg
phi(turb)	Yaw angle	deg
omega	RPM	rpm
theta1	Blade 1 Pitch Angle	
	(Digital Blade 1 pitch in Phases III and IV)	deg
theta2	Digital Blade 2 pitch	deg ')
theta3	Digital Blade 3 pitch	deg ')
Power	Generator Power	kW
Abs Ref Press	Absolute reference pressure	Pa ")

') Phase III and Phase IV only.
") Phase II only.

designed to be stiff with a system fundamental frequency exceeding 10 cycles per revolution (10P), and the axes of the boom and camera were mass balanced about the axis of rotation. The camera angle was remotely adjustable to display various span locations on the blade. During all three phases of testing an additional high-shutter-speed video camera was mounted at the root of the instrumented blade to provide a view of the blade span. This camera pitched with the blade to provide a full span picture of all the tufts at one time. The mass of this camera was included in the mass of the blades listed in Appendix E during Phases III and IV. However, during Phase II, the blades were balanced before the camera was mounted. Additional equipment, such as the data acquisition system, the PSC, and lighting for night testing, were also mounted on the hub. Variations in the mass of the hub due to various combinations of this equipment for each phase of the experiment are noted in Appendix E.

4.3.3 Measuring procedure

Data acquisition and measuring speed

A customized digital PCM-based hardware system for data acquisition was developed and tested throughout Phase I of the Combined Experiment (Simms and Butterfield, 1990, [19]). The same hardware was used during Phase II, but upgrades were made for Phases III and IV. The number of measured channels increased from 185 in Phase II to 201 in Phase IV. Throughout Phase II testing, the inflow measurements and the non-rotating turbine measurements were acquired at slower sample rates than that of the rotating measurements. The slower rate channels were interpolated during post-processing to a common 520.83 rate for all channels. During Phases III and IV, all of the channels were sampled at 520.83 Hz. Data were stored on 14-track magnetic tape during Phase II data acquisition, but recent technological advances in personal computing provided the capability for real time data collection and storage on optical disk during Phases III and IV. Copies of the optical disks and the processed engineering unit files were recorded on compact disks for storage.

Preparation of the data provided to the data base required filtration and decimation. The MATLAB program was used to first digitally filter and then decimate the data to a 52 Hz sample rate. Time series data (except azimuth angle and time channels) were passed through a 4-pole Butterworth 10 Hz filter in both forward and backward time directions resulting in 8-pole, 0 phase, 10 Hz Butterworth

filtering. All channels were then decimated by 10 to achieve the resulting 52 Hz sample rate. The effect of applying these filters is illustrated in the figures 4.22 and 4.23.

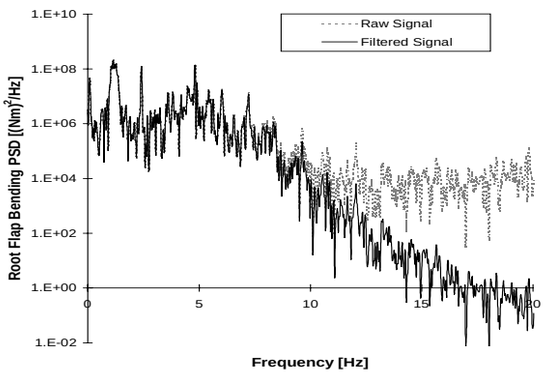

Figure 4.22 *NREL:The effect of applying the filter seen on a power spectrum*

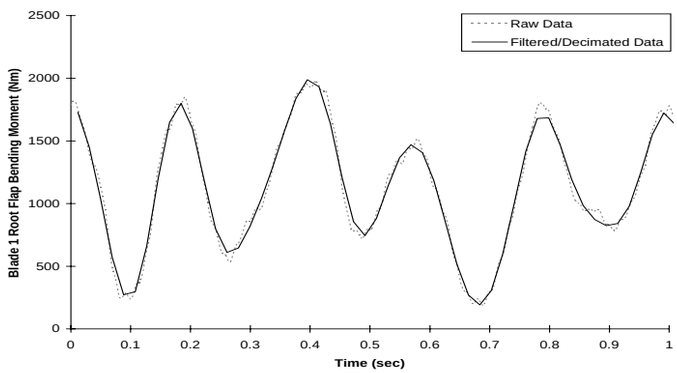

Figure 4.23 *NREL: The effect of applying the filter seen on a time trace*

Calibration Procedures

Calibrations of the pressure channels were performed in the manner described in Simms and Butterfield ([20]) by using a motorized syringe to apply positive and negative pressure to all scanning transducers simultaneously over their entire measurement range. This was done before and after each ten minute campaign by remote control while the turbine was in motion. Calibration coefficients were derived by performing a least-squares regression on each of the pressure channels referenced to the precision differential pressure transducer signal. In order to verify lack of drift in the pressure transducers, comparisons between pre- and post-calibrations were made.

A variety of calibration procedures were used to ensure that the non-pressure channels maintained required accuracy levels. The preferred method of calibrating

Table 4.10 *Uncertainty Analysis Results for Selected Measured Channels*

Measurement	Units	Measurement Range	Total Estimated Uncertainty	% Full Scale Error
Pressures at 30% Span ')	Pa	+/- 2970	+/- 12	0.2
Pressures at 47% Span ')	Pa	+/- 2970	+/- 18	0.3
Pressures at 63% Span ')	Pa	+/- 8274	+/- 33	0.2
Pressures at 80% Span ')	Pa	+/- 8274	+/- 50	0.3
Angle of attack	deg	-22 to +40	+/- 1.0	1.6
Wind velocity	m/s	0 to 37	+/- 0.5	1.4
Blade pitch angle	deg	-10 to 71	+/- 1.0	1.2
Blade azimuth angle	deg	0 to 360	+/- 1.0	2.8

') All pressures are differentials between hub reference and blade surface pressures.

channels in the field was to use an "end-to-end" procedure where a known load was applied and the effect measured. This enabled the full system measurement path to be calibrated. An example is strain gage calibration where weights suspended from the blade caused a known strain gage bending moment. For other channels, it was impossible to perform full-path calibrations in situ. For example, the anemometers required a known wind velocity and were thus calibrated in a wind tunnel. In these cases, a two-part calibration was used. The first part relied on the factory-specified transducer calibration. The second part was an "electronics cal" where known reference voltages were inserted in place of the transducer signal, and the system electronics path was calibrated separately. The frequency of these calibrations depended on transducer and measurement system specifications and varied with use and application.

The calibration procedures were established to ensure that all recorded data values were within the stated error limits. Uncertainty analysis results for selected measured channels used during Phase II are presented in table 4.10, (from Miller et al., Unpublished, [21]). Total estimated uncertainty values listed in the table are expressed in engineering units, and represent random and bias error components. The uncertainty is also expressed in terms of percent full scale error. Detailed measurement uncertainty estimates for Phase II data channels can be found in Butterfield et al. ([15]). Error analysis and calibration procedures specific to wind turbine field testing are described in McNiff and Simms ([22]).

A data base of resulting calibration coefficients was maintained and applied to raw data values to produce engineering unit data files. Because all of the measured channels were linear, only slope and offset calibration coefficients were applied.

Surface pressures

Differential pressures between the blade surface pressure and the hub reference pressure were measured by the ESP-32 pressure transducers. For all blade surface pressure measurements, the common reference pressure source was the pressure inside one of the rotating instrumentation boxes on the hub. The reference tap of each transducer was connected to a single reference line that was terminated inside the instrumentation box. The hub mounted instrumentation box was damped to atmospheric pressure through an orifice which resulted in a time constant of approximately 5-10 seconds. This damping provided a relatively stable pressure reference which closely tracked atmospheric pressure. The effects of centrifugal

force on air in the tube were corrected per equations 4.5 and 4.6 as described in Miller et al, [21].

$$p_{cor} = p_{meas} + p_{cent} \tag{4.5}$$

$$p_{cent} = 0.5\rho(\Omega \cdot r)^2 \tag{4.6}$$

where
p_{cor} = differential pressure corrected for centrifugal force, Pa
p_{meas} = pressure differential measured at blade-mounted transducer, Pa
p_{cent} = centrifugal force correction, Pa
ρ = air density, kg/m^3
r = radial distance to surface pressure tap, m
Ω = rotor speed, rad/s

The associated pressure files in the data base contain p_{cor}–the measured difference in pressure between the surface tap pressure and the hub pressure corrected for effects of centrifugal force. If a pressure tube was damaged, the interpolated value between the two adjoining taps was calculated. These channels were noted as P(deriv) in the log files to indicate interpolation instead of actual measurement. A separate file for each of the full chord span locations (30%, 47%, 63%, 80%, and 95%) as well as each of the intermediate span locations (36%, 41%, 52%, 58%, 69%, 74%, 85%, 90%, 92%, and 98%) was placed in the data base.

Dynamic Pressure

A total pressure Pitot probe attached to the local flow angle flag pictured in figure 4.20 measured dynamic pressure during Phases II and III. To prevent flow disturbance, the probe extended 0.64 m (0.62 m during Phase II) ahead of the leading edge of the airfoil and was mounted 4% outboard of each primary pressure station (30%, 47%, 63%, and 80%). Again, the probe was mounted at 86% span instead of 84% span during Phase II. Each probe was connected to an ESP-32 transducer via 0.15 cm diameter stainless steel tubing. A short piece of plastic tubing was used to join the tubes to the transducer. The probes measured the difference between the stagnation and reference pressures with less than 10% error for inflow angles between -40 deg and 40 deg ([23]). To maximize the probe's effectiveness, they were bent so the measurement range would coincide with the nominal operating conditions. During Phase IV the five-hole probe provided a dynamic pressure measurement 0.36 m ahead of the leading edge at an angle of 20 deg below the chordline. The five-hole probes were mounted in the same locations as the total pressure probes with the addition of one at 91% span. The dynamic pressure was corrected for centrifugal effects in the same manner as the individual pressure taps using equations 4.5 and 4.6.

The dynamic pressure was also estimated from the stagnation point pressure at each of the full-chord pressure tap locations. The location on the blade at which the local velocity equals zero was considered to be the stagnation point, and the corresponding pressure at that location was used as the stagnation pressure. The resolution of the pressure taps on the lower surface was assumed sufficient to extract the maximum positive surface pressure, especially at lower angles of attack where the stagnation point was near the leading edge. According to Shipley et al. ([24]) the stagnation point normalization method is the preferred method of

Table 4.11 *Dynamic Pressure Measurements*

Identification	Description	Units
q(stag,1)	Stagnation Pressure at 30% span	Pa
q(stag,4)	Stagnation Pressure at 47% span	Pa
q(stag,7)	Stagnation Pressure at 63% span	Pa
q(stag,10)	Stagnation Pressure at 80% span	Pa
q(stag,14)	Stagnation Pressure at 95% span	Pa
q(dyn,34)	Dynamic Pressure, 34% span	Pa
q(dyn,51)	Dynamic Pressure, 51% span	Pa
q(dyn,67)	Dynamic Pressure, 67% span	Pa
q(dyn,84)	Dynamic Pressure, 84% span	Pa ')
q(dyn,86)	Dynamic Pressure, 86% span	Pa ")
q(dyn,91)	Dynamic Pressure, 91% span	Pa ')

") Phase II only.
') Phase III and IV only.

estimating dynamic pressure on the blade. Dynamic pressure measurements are listed in table 4.11.

Force coefficients
Each of the measured blade surface pressure values was normalized by the stagnation pressure at the corresponding span location as shown in equation 4.7.

$$C_p = \frac{p_{cor}}{q_{stag}} \tag{4.7}$$

where
C_p = normalized pressure coefficient, dimensionless
p_{cor} = differential pressure corrected for centrifugal force, Pa
q_{stag} = stagnation point dynamic pressure (corrected for centrifugal force), Pa.

The pressure distributions for rotating-blade data were integrated to compute normal force coefficients (c_n) and tangent force coefficients (c_t) per unit length. These are fundamental coefficients that are commonly used to describe airfoil performance from pressure measurements because their derivation is independent of the angle-of-attack measurement. They represent the forces acting perpendicular and parallel to the airfoil chord, respectively. The average pressure between two adjacent taps was first projected onto the chord line, integrated to determine the c_n values, and then projected onto an axis orthogonal to the chord and integrated to compute c_t values. This procedure is described in detail by [25]. Equations 4.8 and 4.9 give the integration procedure used to determine c_n and c_t. The x and y values begin at the trailing edge, cover the bottom surface of the blade, and then the top surface, ending at the starting point, the trailing edge.

$$c_n = \sum_{i=1}^{nr.taps} \frac{C_{p,i} + C_{p,i+1}}{2}(x_{i+1} - x_i) \tag{4.8}$$

$$c_t = \sum_{i=1}^{nr.taps} \frac{C_{p,i} + C_{p,i+1}}{2}(y_{i+1} - y_i) \tag{4.9}$$

where,
C_p = normalized pressure coefficient
x_i = distance along chord line from leading edge to i^{th} pressure tap
y_i = distance from chord line along axis orthogonal to chord to i^{th} pressure tap

In a similar integral procedure, pitching moment coefficients (c_m) were determined. The pitching moment represents the total moment about the pitch axis (1/4 chord) due to the normal and tangential forces at a pressure tap with the vertical or horizontal distance from the pitch axis as the moment arm. This equation is given in 4.10:

$$c_m = \sum_{i=1}^{nr.taps} \frac{C_{p,i} + C_{p,i+1}}{2}(x_{i+1} - x_i)(\frac{x_{i+1} - x_i}{2} + x_i - 0.25)$$

$$+ \sum_{i=1}^{nr.taps} \frac{C_{p,i} + C_{p,i+1}}{2}(y_{i+1} - y_i)(\frac{y_{i+1} - y_i}{2} + y_i) \quad (4.10)$$

All other airfoil performance coefficients, such as lift (c_l), pressure drag (c_{dp}), torque (c_{torque}), and thrust (c_{thrust}), were computed using the c_n and c_t values in conjunction with their reference angles. Torque and thrust coefficients were calculated as a function of blade pitch angle (ϕ) and local twist angle (β), both of which were easily measured. Lift and pressure drag coefficients, on the other hand, rely upon the angle of attack (α) which is not as easily acquired. For this reason, only torque and thrust coefficients were included in the data base, but the equations used to determine lift and pressure drag coefficients are shown in the equations 4.11 to 4.14.

$$c_{torque} = c_n \sin(\phi + \beta) + c_t \cos(\phi + \beta) \quad (4.11)$$

$$c_{thrust} = c_n \sin(\phi + \beta) - c_t \cos(\phi + \beta) \quad (4.12)$$

$$c_l = c_n \sin(\alpha) + c_t \cos(\alpha) \quad (4.13)$$

$$c_{dp} = c_n \sin(\alpha) - c_t \cos(\alpha) \quad (4.14)$$

Torque and thrust coefficients were integrated along the span of the blade and multiplied by the number of blades to provide a rough estimate of the total aerodynamic thrust and torque applied to the entire rotor. All of the aerodynamic force coefficients included in the data base are listed in table 4.12. The estimated aerodynamic thrust and torque appeared with the turbine load measurements in table 4.7 for Phase II and table 4.8 for Phases III and IV.

Angle of Attack
Wind tunnel tests were performed with the flag sensor mounted on a full-chord scale airfoil section in order to develop a correction for upwash and to determine the dynamic characteristics of the flag. The configuration and resulting data are explained in the Phase I report (Butterfield et al., [15]). The upwash correction derived from wind tunnel testing was applied to all of the local flow angle measurements, including those made with the five-hole probes, as 4.15.

$$\alpha = 5.427 \cdot 10^{-5} \cdot \alpha_m^3 + 6.713 \cdot 10^{-3} \cdot \alpha_m^2 + 0.617 \cdot \alpha_m + 0.8293 \quad (4.15)$$

Table 4.12 *Force coefficients*

Identification	Description	Units
cn1	Normal force at 30% span	Cn
cn4	Normal force at 47% span	Cn
cn7	Normal force at 63% span	Cn
cn10	Normal force at 80% span	Cn
cn14	Normal force at 95% span	Cn ')
ct1	Tangent force at 30% span	Ct
ct4	Tangent force at 47% span	Ct
ct7	Tangent force at 63% span	Ct
ct10	Tangent force at 80% span	Ct
ct14	Tangent force at 95% span	Ct ')
cth1	Thrust Coefficient at 30% span	Cth
cth4	Thrust Coefficient at 47% span	Cth
cth7	Thrust Coefficient at 63% span	Cth
cth10	Thrust Coefficient at 80% span	Cth
cth14	Thrust Coefficient at 95% span	Cth ')
ctq1	Torque Coefficient at 30% span	Ctq
ctq4	Torque Coefficient at 47% span	Ctq
ctq7	Torque Coefficient at 63% span	Ctq
ctq10	Torque Coefficient at 80% span	Ctq
ctq14	Torque Coefficient at 95% span	Ctq ')
cm1	Pitch Moment Coefficient at 30% span	Cm
cm4	Pitch Moment Coefficient at 47% span	Cm
cm7	Pitch Moment Coefficient at 63% span	Cm
cm10	Pitch Moment Coefficient at 80% span	Cm
cm14	Pitch Moment Coefficient at 95% span	Cm ')

') Phases III and IV only.

Table 4.13 *Phase II and Phase III Upwash Corrected LFA Measurements*

Identification	Description	Units
alpha(c,1)	AOA 30% span (upwash corrected)	deg
alpha(c,4)	AOA 47% span (upwash corrected)	deg ')
alpha(c,7)	AOA 63% span (upwash corrected)	deg
alpha(c,10)	AOA 80% span (upwash corrected)	deg

') Appears in Phase III only.

Table 4.14 *Phase IV Upwash Corrected LFA and Crossflow Angle Measurements*

Identification	Description	Units
alpha(c,34)	AOA 34% span (upwash corrected)	deg
alpha(c,51)	AOA 51% span (upwash corrected)	deg
alpha(c,67)	AOA 67% span (upwash corrected)	deg
alpha(c,84)	AOA 84% span (upwash corrected)	deg
alpha(c,91)	AOA 91% span (upwash corrected)	deg

where
α = upwash corrected angle of attack, deg
α_m = local flow angle measurement, deg

This upwash correction has proven satisfactory in displaying aerodynamic performance (Simms, Robinson, Hand, and Fingersh, [26]) for measurements made with the flag sensor, but confidence in this application of the upwash correction to the five-hole probe measurements has not yet been achieved. Both the local flow angle measurement and the upwash corrected result were included in the data base files. Channels associated with upwash corrected angle of attack for each phase of testing are listed in the tables 4.13 and 4.14.

Other Derived Channels

A sonic anemometer was used to measure wind velocity and direction in the u, v, and w orthogonal component directions. These vector components were transformed into magnitude and direction during post-processing. Only the resultant magnitude and direction were included in the data base files.

The Richardson number provides an indication of atmospheric stability based on temperature gradients and wind shear. This was calculated using the equations 4.16 to 4.18 and was included in the data base for all campaigns.

$$\mathrm{Ri} = \frac{\left(\frac{9.8}{\Theta_m}\right)\left(\frac{\Delta\Theta}{\Delta Z}\right)}{\overline{V^2_{shear}}} \tag{4.16}$$

$$\Theta = T\frac{100,000}{P}^{0.286} \tag{4.17}$$

$$V_{shear} = \frac{\sum_{n=1}^{N-1} \frac{WS_{n+1}-WS_n}{Z_n+1-Z_n}}{N-1} \tag{4.18}$$

where

Ri = Richardson Number, dimensionless
Θ_m = Average Potential Temperature between top and bottom of tower, K

$\Delta\Theta$ = Potential Temperature difference between top and bottom of tower, K
ΔZ = Elevation difference between temperature measurements, m
V_{shear} = Average vertical wind shear over ΔZ, m/s/m
Θ = Potential temperature, K
T = Measured, dry-bulb temperature, K
P = Barometric pressure, Pa
N = Number of wind speed measurements
WS_n = Wind speed, m/s
Z_n = Elevation at n^{th} wind speed measurement, m

4.4 RISØ test turbine

The design and construction of the experimental facility was initiated back in 1987 funded by the Danish Ministry of energy and the DGXII research programme of The European Union. In 1989 the first measurement programme was carried out followed by new measurement campaigns in 1991, 1992 and 1993. Then in 1994 the facility was closed down.

4.4.1 Global characteristics of facility

The facility was developed to provide experimental results that could be used to identify the main mechanisms controlling the aerodynamic forces on a rotating HAWT blade in natural conditions. In particular, the measurements were carried out for use in quantifying the importance of 3D flow effects, unsteady effects and rotary wing effects on a stall regulated rotor. A detailed description of the facility and the experimental results can be found in the references [27], [28] and [29].

The key feature of the facility is a system that enables the measurement on the rotating blade of the local aerodynamic forces and the local inflow to the blade. On basis of such measured quantities the airfoil characteristics c_l and c_d as function of instantaneous angle of attack α can be derived for the rotating blade at different spanwise stations and compared with conventional 2D airfoil data.

The measurements have been carried out on the 100 kW Tellus machine at the wind turbine test site at Riso. It is a fixed pitch, stall controlled, three bladed turbine, see figure 4.25. The turbine has a double wound generator which gives the following two synchronous rotational rotor speeds:

- 47.5 rpm, 47.9 rpm at rated power
- 35.6 rpm, 36.3 rpm at rated power

The tower is of the lattice type with three main tower poles and its height is 29.3 m. The blade type is the LM 8.2 m blade which has both twist and taper, see figure 4.24.

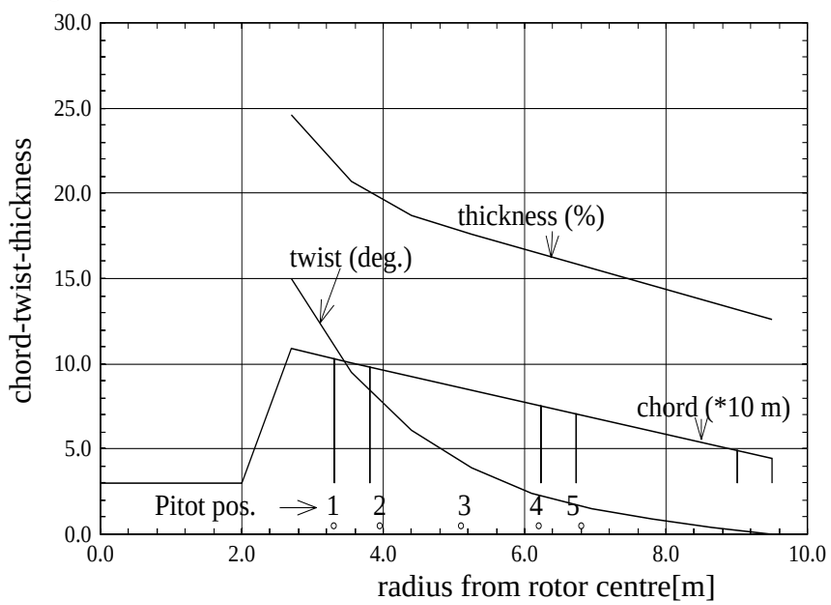

Figure 4.24 *RISØ, The planform data for the test blade including positions of the three blade segments and the positions for the attachment holes for the pitot tube*

Figure 4.25 *The 100 kW stall regulated wind turbine used for the RISØ experiments*

A few data on the turbine are listed below:

Rotor:
- Hub height: 29.3 m
- Number of blades: 3
- Rotor diameter: 19.0 m
- Swept area: 284 m^2
- Tilt: 5 deg
- Coning: 0 deg
- Blade tip angle (measured):
  - 1.8 deg
  - 1.8 deg
  - 1.5 deg
- Power control: stall
- Direction of rotor rotation (seen in front): anti-clockwise

Blades:
- Type: LM-Glasfiber 8.2 m, cantilevered GRP
- Spar material: GRP
- Shell material: GRP
- Blade length: 8.2 m
- Profiled blade length: 6.8 m
- Blade extensions: 1 m
- Root chord: 1.09 m
- Tip chord: 0.45 m
- Blade twist: 15 deg
- Blade profile: NACA 63n-2nn series
- Air brakes: Spoilers positioned on the suction side

Gearbox
- Gear ratio: 1:21.063

Location
The test site is situated at Riso on the east side of Roskilde Fjord running approximately south - north. The inflow conditions depend strongly on the wind direction with low turbulence intensities for west to north west directions whereas high turbulence intensities are found for most of the other directions.

4.4.2 Instrumentation

Blade instrumentation
One of the blades has been modified so that the aerodynamic forces on three segments of the blades can be measured, see figure 4.26. Each blade segment is 0.5 m in spanwise length and is suspended on a 3 component balance attached to the main spar of the blade, see figure 4.28.

The force components measured on each balance is the normal force N, the chordwise force T and the pitching moment M. The radial positions of the mid of the blade segments are the following, see figure 4.27

Segment 1:	Radius 3.56 m,	37 % radius
Segment 2:	Radius 6.48 m,	68 % radius
Segment 3:	Radius 9.26 m,	98 % radius

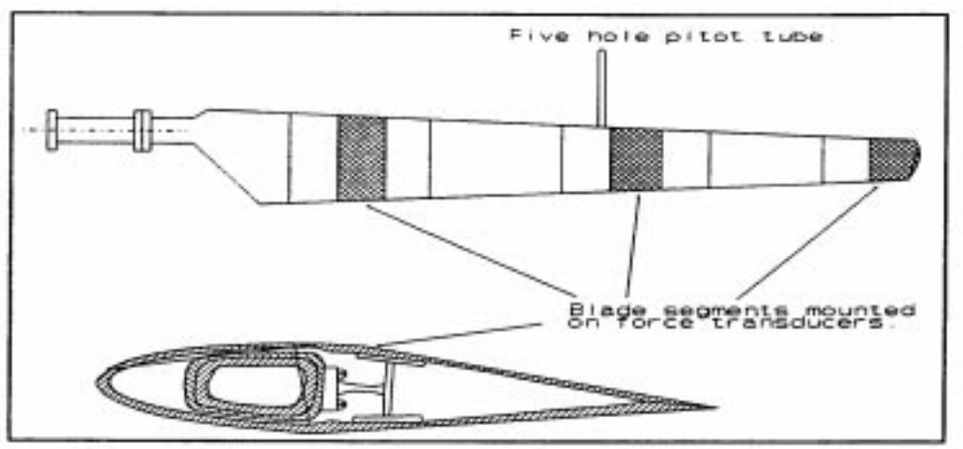

Figure 4.26 *RISØ, The principal layout of the test blade with the three blade segments and the pitot tube for measuring the inflow*

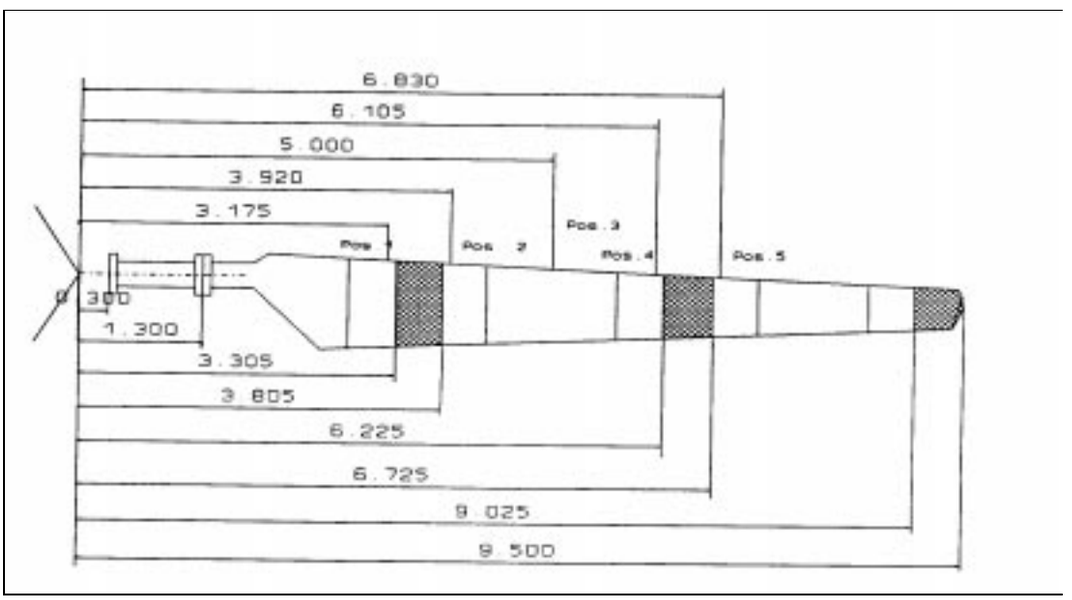

Figure 4.27 *The geometry data for the test blade. Positions for the pitot tube are shown on the upper part of the picture and blade segments on the lower part*

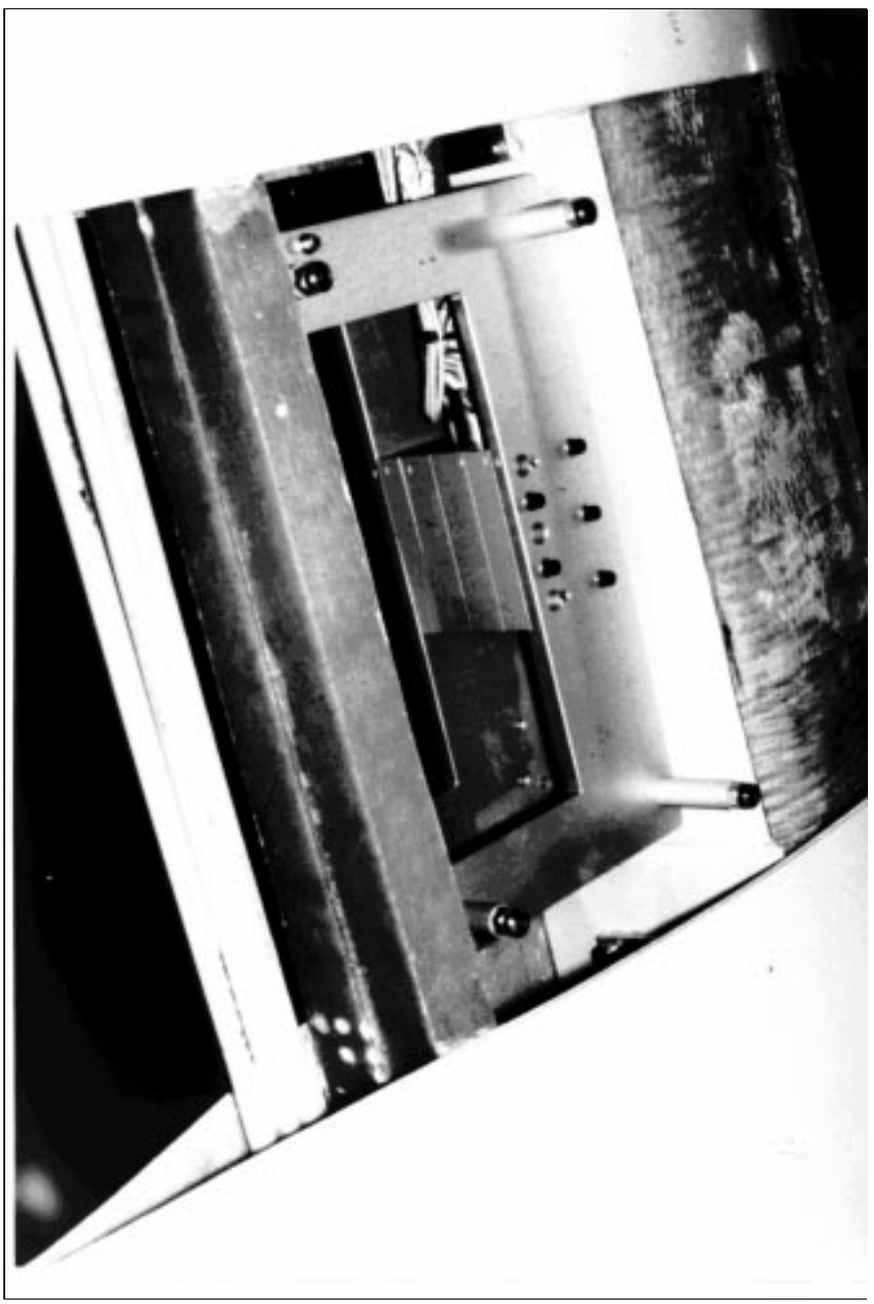

Figure 4.28 *RISØ, The balance and the supporting structure for one of the blade segments*

In order to derive the aerodynamic force component from the total measured force the inertial force component must be subtracted. This is done on basis of a measurement of the acceleration of each of the balance attachments to the main blade, see figure 4.29. The inflow to the blade has been measured with a five hole

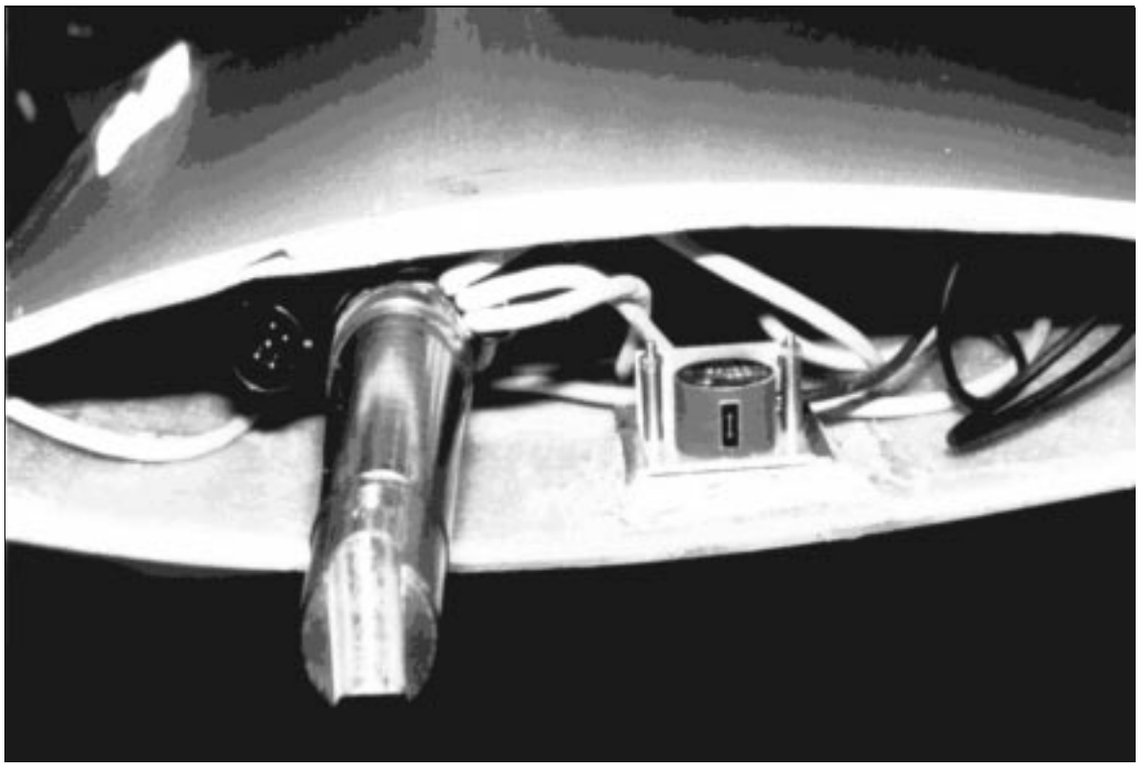

Figure 4.29 *RISØ, The balance for the blade tip segment and the accelerometer to measure flapwise acceleration in order to compensate for the structural force component in the total measured force*

pitot tube mounted on the blade about one chord length in front of the leading edge of the blade, see figure 4.30. The pitot tube can be positioned at different radial positions as marked on figure 4.27, but for all the measurements supplied to the IEA data base the pitot has been in position 5 which is just outboard the mid blade segment. The four pressure transducers for the pitot tube were build into the blade close to pitot tube so that the length of the flexible tubes was around 1.5 m.

Additional signals

The flapwise blade root moment was measured on all three blades. On the turbine the main shaft torque, rotational speed, electrical power, rotor position and yaw position was measured. In the meteorological tower placed about two turbine diameters to the west, wind speed and wind direction was measured at hub height. At the ground air temperature and air pressure was measured

4.4.3 Measuring speed

The complete data acquisition system was configured with the measurements from the meteorology mast and the wind turbine connected to a PC. The sensors were

Figure 4.30 *RISØ, The five hole pitot tube measuring the inflow velocity vector to the blade*

supplied with 15 V and the signals are transferred with a voltage range from -5V to +5V. A 16 channel telemetry system was mounted on the rotor and the data were transmitted to the ground as PCM signals.

All the channels pass through a filter that protects the equipment from lightning. Before the digital sampling, the signals pass through an anti aliasing filter with a cut off frequency of 20 Hz. The sampling frequency for all channels was 25 Hz. Each measurement period is 10 min. and the data are kept as binary files in the form of time series.

4.4.4 Data reduction

All the data signals except rotor position are as a first step in the data processing filtered with a digital low pass filter with a cut off frequency between 2.5 and 3 Hz. The effect of this filtering is illustrated in figure 4.31 and 4.32

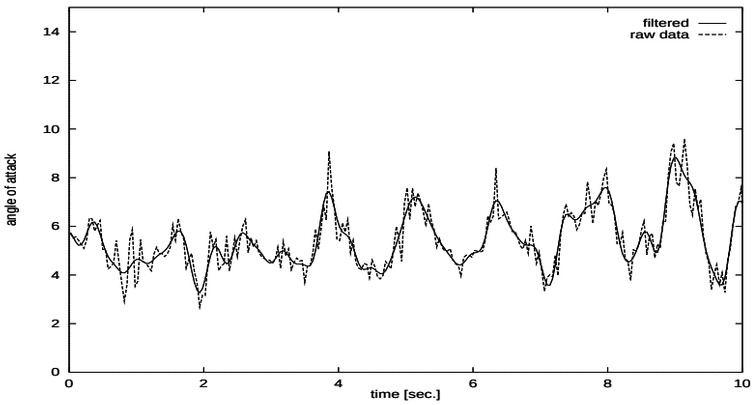

Figure 4.31 *RISØ:The effect of applying the filter seen on a time trace of the measured angle of attack*

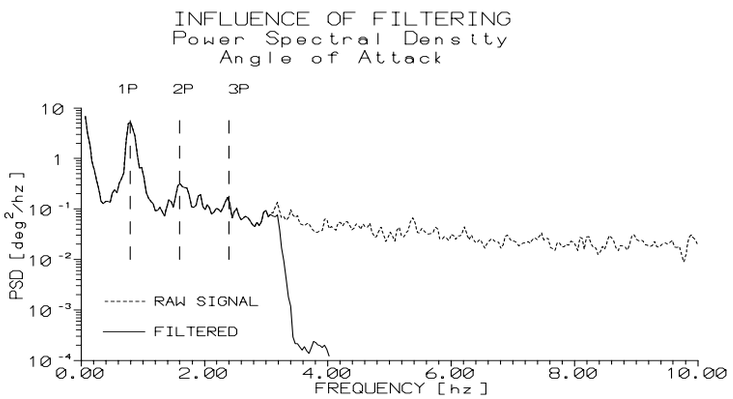

Figure 4.32 *RISØ: The effect of applying the filter seen on a power spectrum of the measured angle of attack*

The measured angle of attack and the relative velocity W_{pitot} are derived from the four measured pressure signals on the five hole pitot tube on the basis of calibrations in a wind tunnel. To derive the airfoil characteristics for the different blade segments W_{pitot} is scaled with the radius ratio between the pitot position and the radial position of the mid of the segment:

$$W_{segment} = W_{pitot} \cdot \left(\frac{r_{segment}}{r_{pitot}}\right)$$

A thorough discussion of the correction of the measured angle of attack with the pitot tube α_{pitot} is presented in [27]. Shortly, the objective with the correction is to achieve the same relation between angle of attack and rotor power as computed with the blade element momentum (BEM) theory below stall so that the measured airfoil characteristics can be used for rotor computations with this code.

The correction is simply a constant which is subtracted the measured angle of attack:

$$\alpha_{\mathrm{segment}} = \alpha_{\mathrm{pitot}} - 4.7[^{\circ}]$$

The airfoil coefficients $c_{n,i}$ and $c_{t,i}$ at segment i are now derived as:

$$c_{n,i} = \frac{N_i}{0.5\rho W_i^2 c_i l_i}$$

$$c_{t,i} = \frac{T_i}{0.5\rho W_i^2 c_i l_i}$$

where l_i is the spanwise length of the segment, N_i and T_i are the measured normal and tangential aerodynamic force on the segment, W_i the corrected inflow velocity as shown above and c_i is the chord on the mid of the segment.

4.5 DUT test turbine

For a very detailed description of the DUT facility reference is made to [30].

4.5.1 Global characteristics of facility

Figure 4.33 *DUT test facility*

- Blade: Prince Fiber Technics (Aerpac) mounted on an experimental turbine, see figure 4.33.
- Number of blades: 2
- Blade span (from flange to tip) = 4.4 m
- Rotor diameter = 10 m
- Blade profile: NLF(1)-0416
- Blade without twist and taper
- Pressure tap measurements around profiles at 4 different radial stations, see figure 4.34.
- The inflow velocity is measured with a pitot probe, see figure 4.34. The inflow angle is measured with a three hole probe mounted at 75% span. The length of this probe is 0.55c and the angle between the probe and the chord is 0 deg.

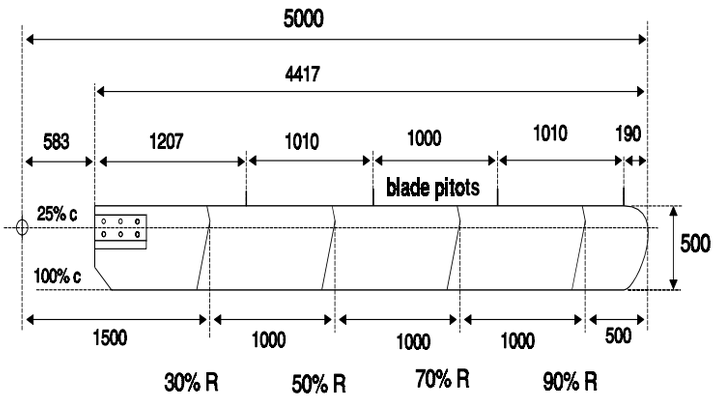

Figure 4.34 *DUT: Drawing of the instrumented blad with 4 spanwise locations of the pressure taps and the four blade pitots. The three hole flow direction probe wa located at the 75% spanwise position*

Location

The Open Air Rotor Research Facility is located at the Delft University of Technology near Delft in the Netherlands. Figure 4.35 gives a map of the site and environment. The prevailing wind direction is from South-West. A roughness hight of 0.25m was assumed. The turbulence level is not yet determined.

4.5.2 Instrumentation

- Pressure taps at 4 rotor blade sections, These taps are positioned at 30%, 50%, 70% and 90% of the rotor radius.
  Note that the sections are not measured simultaneously. In the present project, measurements from the 70% station have been supplied.
  There are 59 taps per station with 0.4 mm diameter, see the figures 4.36 to 4.39.
- A 3 hole probe is mounted at the 75% span location
- All signals from the rotor are transferred via sliprings. The voltage output from the transducers is transferred to current to reduce the variable resistance effects of the sliprings. The strain gauge signals from the hub are pulse coded before they are transmitted over the sliprings. Table 4.15 summarizes all the collected signals.
- Pressure System:
  The pressures were recorded with two high speed differential electronic transducers from Pressure System Incorporation, type Nr. ESP-32TL. One has a range of $\pm$ 1 Psi ($\pm$ 7000 Pa), the other has a range of $\pm$ 2.5 Psi (($\pm$ 17000 Pa) Each transducer has 32 ports and a built-in calibration facility. The reference port of the transducers was via a damper connected to a Kiel pitot tube on the hub. To obtain the static reference pressure this total pressure is numerically corrected with the dynamic pressure of the wind. The damper was placed close to the reference port of the transducers in the blade. A special designed three

Figure 4.35 *DUT: Map of the Open Air Rotor Research Facility and environment. The hight of the most important structures (trees) are given in meters on the drawing. The arrow denotes the North direction. The two circles indicate a distance of 100m and 250m respectively*

hole probe was used to measure the flow direction near the 70% radial section. Pulse tests were carried out to check the acoustic behaviour of the pressure tube systems. Maximum frequency response of a pressure port is several tens Hz.

- Damper:
  The reference port and the measurement ports of the transducers showed a different dynamic response. Therefore a damper was installed to make a numerical correction possible for the variation of the static pressure created by the vertical movement of the transducers (altitude effect). This pressure variation did not cancel out due the different dynamic response of the reference port and the measurement ports. The damper RC time was adjusted to 2.1 s. To avoid different behavior in dynamic response the pressure taps were connected to identical tubes of 70cm length and an inside diameter of 2mm for the brass tubes, and 1 mm for the flexible tubes.
- Wind Measurement:
  The wind speed and wind direction were measured with a Sonic wind meter on a mobile tower one rotor diameter upstream at hub axis height. In addition a

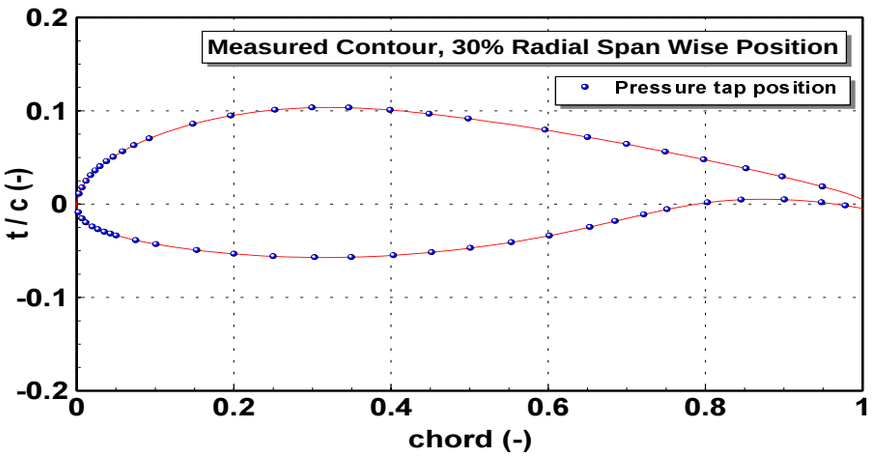

Figure 4.36 *DUT: Position of pressure taps on measured contour of the 30% radial spanwise section smoothed with XFOIL to reduce the effects of the inaccuracy of the contour measurement method*

cup anemometer was used at nearly the same position.

- Flow Patterns
  The flow pattern on the blade suction side surface was visualized with tufts. A rotating micro video camera, mounted near the hub, recorded the picture of these tufts. This picture was overlayed directly during the data acquisition with graphs of the pressure distribution ($C_p - x$) and other measurement data of interest. A special video overlay board was therefore installed in the PC-based data acquisition system.
- PC-based Data Acquisition System
  A 80486 PC runs the special custom written data acquisition software. The data acquisition software is written in Borland C++. The PC is equipped with an Advantech PCL818 100Khz 16 channel data 12 bits AD acquisition board. The Advantech board controls also the addressing lines of the multiplexed pressure transducers. A special hold switch in the transducer output lines speeds up the pressure measurements: the next pressure port is already addressed while the computer digitizes the previous pressure port. This reduces the settling time of the electronics. A Magni VGA Producer Pro board overlays the camera video signals with the screen output from the computer and sends the result to a standard S-VHS video recorder. The data acquisition software has the capacity to process and to display directly the data in a very flexible way. Only the original non corrected direct digitized values of each channel are stored with the calibration coefficient separate in the file header. A special replay function in the software allows to watch the collected data later in the same way as during the acquisition. During the process of collecting data and replay of the existing data files all the pressures and aerodynamic quantities are calculated from these rough data values.

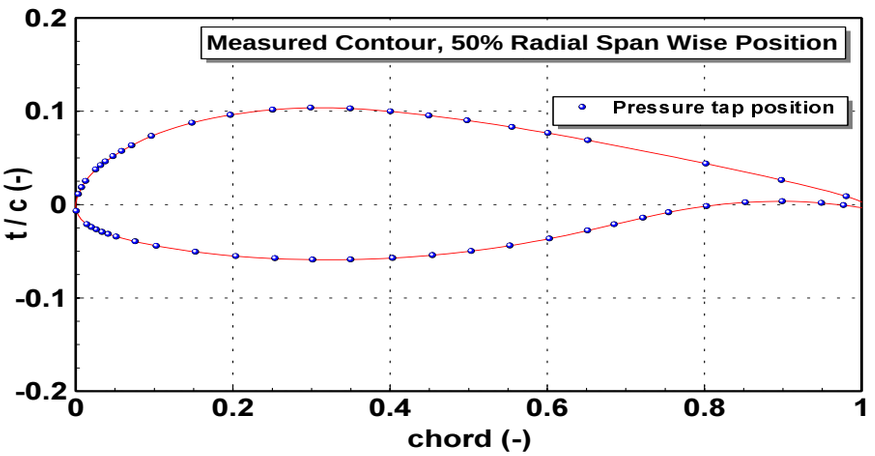

Figure 4.37 *DUT: Position of pressure taps on measured contour of the 50% radial spanwise section smoothed with XFOIL to reduce the effects of the inaccuracy of the contour measurement method*

Table 4.15 *Overview of collected and used instruments*

SIGNALS	INSTRUMENT
pressure taps on the blade, Kiel pitot tubes, three hole flow direction probe	PSI differential pressure transducers
wind speed	cup anemometer at a mobile tower
wind speed and wind direction	Gill Sonic wind meter at a mobile tower
temperature of transducers	PT 100 temperature sensor at transducer
blade flapping moments	strain gauges at the hub
tower bending moments	strain gauges at the tower
picture of tufts	rotating micro video camera at the hub
rotor torque	torque meter at the low speed shaft
rotor speed	tacho generator at generator, from six
azimuth position	degree azimuth pulse from one pulse per revolution

4.5.3 Measurement Speed

All data channels were sampled at 333 Hz. These data readings were averaged directly on line in the memory of the data acquisition computer. The rotational speed of the rotor dictated how many readings were averaged: at every six degrees an averaged value of each data channel was recorded in the file. So the sampling rate of the stored data is 60 times the rotational speed. To reduce the electronic scatter the data was averaged.

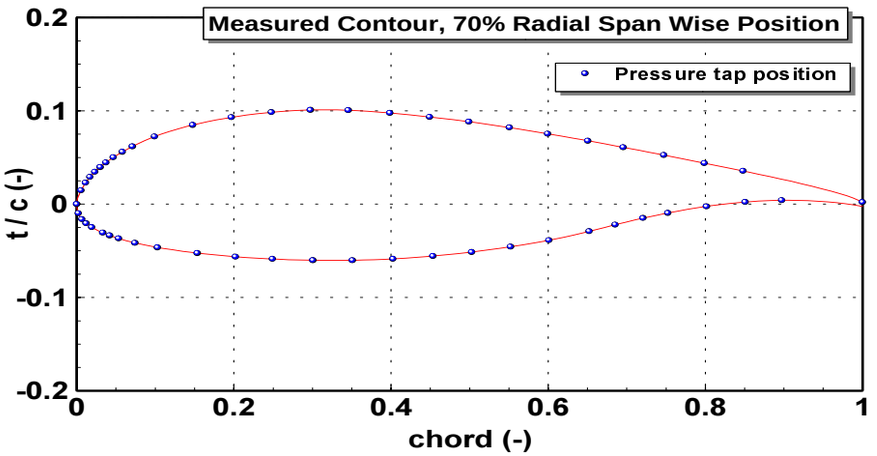

Figure 4.38 *DUT: Position of pressure taps on measured contour of the 70% radial spanwise section smoothed with XFOIL to reduce the effects of the inaccuracy of the contour measurement method*

4.5.4 Calibration procedures

For every measurement series the pressure transducers were manually calibrated by applying six calibration pressures. The transducers have a built-in switch for switching between calibration mode and measurement mode. When the calibration was completed while the turbine was lowered on the ground, the turbine was erected in a few minutes. Each measurement port has its own calibration curve, which is a third degree polynom. The temperature of the transducers has an important influence on the calibration curves. In [31] the different influences on the calibration in relation to the accuracy of the pressure measurements are analyzed.

4.5.5 Data Reduction

For a more detailed description of the pressure correction formulae with the derivations, reference is made to appendix B of [30].

Pressure Data Correction

Three corrections on the pressure signals were employed:

1. a correction on the reference channel with the dynamic pressure $0.5\rho \mathrm{V}^2$ of the wind speed (V), calculated from the wind meter signal. This correction is small but necessary, because the reference port is connected to a total Kiel pressure probe at the hub and not to an atmospheric static probe;
2. an individual centrifugal force correction on each pressure port. The radial position of the pressure tap $\mathrm{r}_{\mathrm{tap}}$ determines the size of this centrifugal force correction;
3. a harmonic altitude correction. This correction is necessary because the reference port is stabilized as much as possible with a damper near the transducers in the reference tube. The amplitude of this effect is mainly determined by the

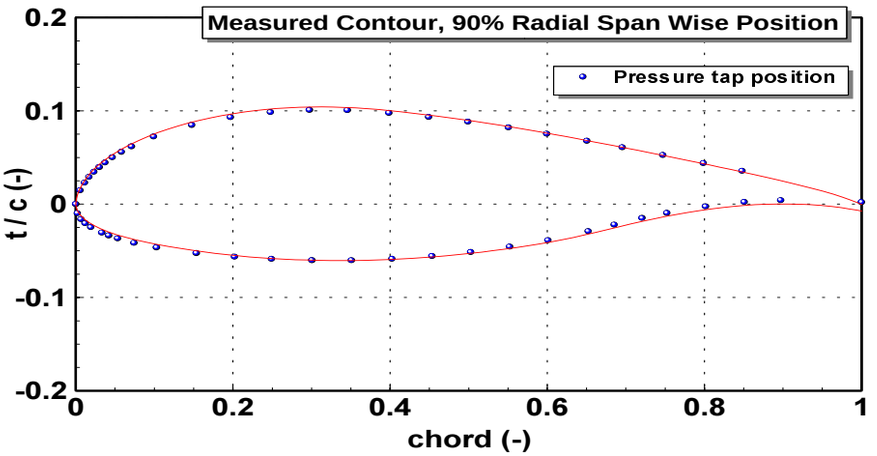

Figure 4.39 *DUT: Position of pressure taps on measured contour of the 90% radial spanwise section smoothed with XFOIL to reduce the effects of the inaccuracy of the contour measurement method*

radial location of the transducers. The correction (amplitude $\delta p_{harmonic}$ and phase ψ) was empirically fitted in such a way, that the value of the pressure coefficient C_p became nearly constant of the tap at the pressure side at 85% chord position. This location was chosen because wind tunnel measurements showed for this tap a nearly constant C_p value for a quite large range of angles of attack. The corrections are calculated on line during the data collection and again during the data replay, since only the non corrected data values were stored.

Calculation of C_p
The pressure coefficient C_p is defined as:

$$C_p = \frac{p_{tap} - p_{atm}}{q} = \frac{p_{tap} - p_{atm}}{p_{pt} - p_{atm}} \tag{4.19}$$

p_{tap} denotes the static pressure of a tap, p_{atm} is the atmospheric pressure, p_{pt} is the total pressure and q is the dynamic pressure. It was assumed that the static pressure did not differ from the p_{atm}. With the three corrections mentioned in the previous section 4.5.5 C_p was calculated finally with the formula:

$$C_p = \frac{\delta p_{tap} + 0.5\Omega^2 r_{tap}^2 + 0.5\rho V^2 - \delta p_{harmonic}\cos(\Omega t + \psi)}{\delta p_{pt} + 0.5\Omega^2 r_{tap}^2 + 0.5\rho V^2 - \delta p_{harmonic}\cos(\Omega t + \psi)} \tag{4.20}$$

δp_{tap} is the recorded value at the transducer port from a tap and δp_{pt} denotes the recorded value at the transducer port from the total pressure of the blade pitot. V is the undisturbed wind velocity, ρ is the air density and Ω is the rotational speed. The radial position of a pressure tap is r_{tap}.

Calculation of c_n, c_t and c_m
The normal force coefficient c_n, the tangential force coefficient c_t and moment coefficient of a section c_m are obtained directly by integrating the pressure distribution (C_p values) with the trapezium rule. For this calculation the location of the pressure tap nearest to the leading edge was shifted to the leading edge. c_m is calculated at the 25% chord point.

Data Filtering
Until this moment no data filtering with a low pass filter was done. Analysis made by other institutes (RISØ , FFA and ECN) showed that this is a useful technique to smooth the scatter in the experimental data.

Angle of Attack Determination
In section 5, more information is given about the DUT method to determine the angle of attack.

The angle of attack measurements which are performed for IEA Annex XIV are all recorded with a 3 hole probe. A theoretical correction for the 2D upwash and for the effect of finite span and power extraction process has been added.

Wind Tunnel Experiments
In January 1991 the 70% spanwise section was tested in the Low Speed Wind Tunnel of the Aerospace Faculty of the DUT. The tests are described and the results are given in the Appendix A of [32].

4.6 Discussion of differences between facilities

- The diameter of the facilities in the project range between 10 m (NREL, TUD) and 27 m (ECN).
- The number of blade is two (DUT, ECN) or three (NREL, RISØ and IC/RAL).
- The blades of three facilities (ECN, RISØ, IC/RAL) are twisted and tapered. The blades of two facilities (DUT, NREL) are untwisted and untapered. In addition, NREL supplied measurements on a blade which is twisted only.
- The aerodynamic profiles involved in the project are:
  - NACA 44xx (ECN)
  - NACA 632xx (RISØ and IC/RAL)
  - NLF 0416 (DUT)
  - NREL S809 (NREL)
- Most participants measure the pressure distribution around the profiles from which the aerodynamic forces are derived. RISØ measures the aerodynamic forces directly by means of balances, which includes the measurement of the skin friction.
- All participants have instrumented at least three radial stations, i.e. a root station (around 30% span), a mid station (around 60% span) and a tip station (around 80% span). DUT has instrumented 4 stations. NREL has instrumented 4 (Phase II) or 5 (Phase III) stations. IC/RAL has instrumented 6 stations.
- At most facilities the different radial stations were measured simultaneously. At the IC/RAL turbine two stations were measured simultaneously, at the DUT turbine every station was measured separately.
- The IEA Annex XIV measurements of IC/RAL, NREL and RISØ were all made at the same rotor speed and the same pitch angle. The angle of attack was set by means of the wind speed.
- In the DUT IEA Annex XIV experiments the angle of attack was set by means of the rotor speed (and the wind speed).
- In the ECN IEA Annex XIV experiments, the angle of attack is set in various ways; by means of the wind speed, the rotor speed or the pitch angle.
- The number of taps per stations is 25 for IC/RAL, 32 for NREL, 47 for ECN and 59 for DUT, although not all taps were working at the latter.

5. ANGLE OF ATTACK IN FIELD EXPERIMENTS

5.1 General

In aerodynamic field experiments a problem occurs with regard to the definition of angle of attack: Consider a non-rotating blade profile which is placed in a windtunnel. The angle of attack ($\alpha_{0,stat}$) is defined as the angle between the chord and the undisturbed wind vector (denoted by $\overline{V}_{0,\mathrm{stat}}$) which is aligned with the wind tunnel walls. Now suppose that the local inflow angle ($\alpha_{\mathrm{local,stat}}$) is measured ahead of the blade profile with a measuring device (i.e. a 5 hole pitot probe, windvane etc), see figure 5.1.

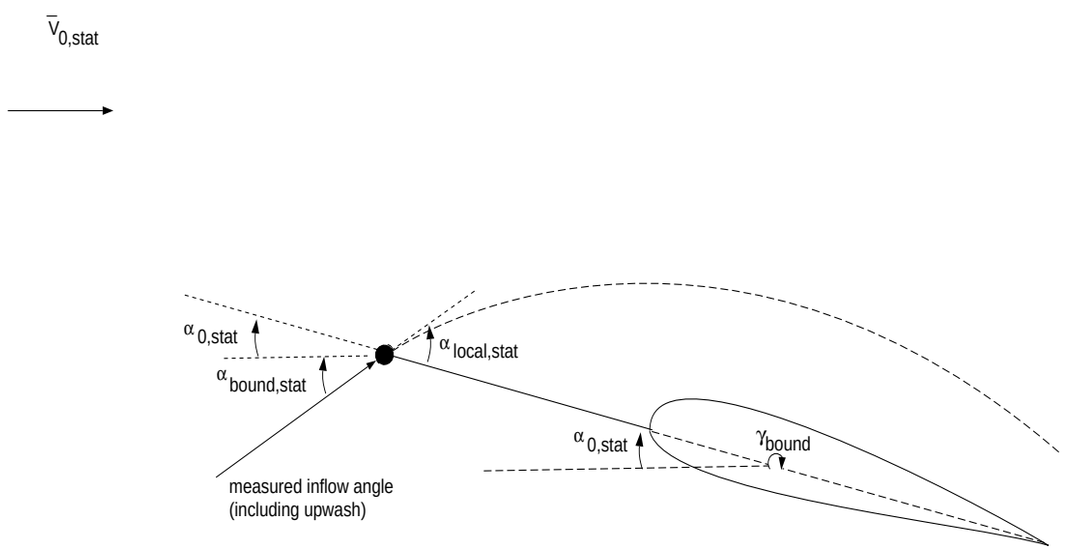

Figure 5.1 *Angle of attack in wind tunnel environment*

Then the angle of attack is related to this local inflow angle by:

$$\alpha_{0,\mathrm{stat}} = \alpha_{\mathrm{local,stat}} - \alpha_{\mathrm{bound,stat}} \tag{5.1}$$

with $\alpha_{bound,stat}$ the upwash angle induced by the bound vorticity. Note that in a windtunnel test under perfect 2D conditions there is no trailing vorticity and consequently, no wake induced velocity.

In a rotating wind turbine environment no such equivalent of $\overline{V}_{0,\mathrm{stat}}$ is known. However in some IEA Annex XIV experiments the local inflow angle ahead of the rotating blade profile ($\alpha_{\mathrm{local,rot}}$) is measured. Then, similar to eqn. 5.1 the upwash induced by the bound vorticity can be substracted:

$$\alpha_{0,\mathrm{rot}} = \alpha_{\mathrm{local,rot}} - \alpha_{\mathrm{bound,rot}} \tag{5.2}$$

This yields the angle of attack between the chord of the blade profile and the effective velocity (V_{eff}), where the effective velocity is composed of the free

stream wind speed (V), the wake induced velocity (u_i) in axial direction and the rotational velocity ($\Omega \cdot r$), see figure 5.2. This hypothetical angle of attack is

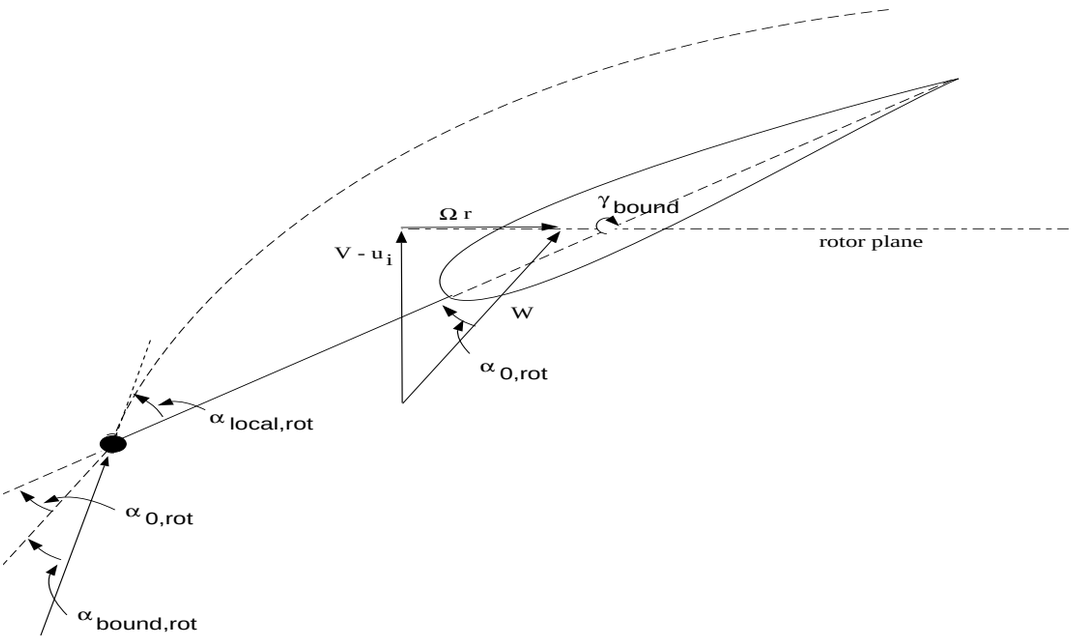

Figure 5.2 *Angle of attack for rotating wind turbine*

commonly used in aerodynamic models for wind turbines. Note that in fact also the wake induced velocity in tangential direction is present in $\alpha_{0,\mathrm{rot}}$. However this value is assumed to be small compared to $\Omega \cdot r$.

In equation 5.2 it is assumed that the wake induced velocity at the measurement point is equal to the value in the rotorplane. Calculations which are described in [33] show that at a position of 0.1 chord length upstream of the rotorplane the wake induced velocity differs $\approx$ 1% from the value in the rotorplane.

5.2 Methods available

Various methods for the determination of the angle of attack ($\alpha_{0,\mathrm{rot}}$) are known.

In this chapter tseveral investigations are summarized, in which different methods for the angle of attack are introduced.

5.2.1 IEA Annex XIV investigation

On behalf of IEA Annex XIV, ECN prepared a document about the angle of attack. This document served as a food for discussion at several project meetings. The methods discussed in the document are mainly based on the methods which are used in the present project. The method applied by IC/RAL is described in section 4.2. The description of this method arrived at the very end of the project and could not be included in the present analysis.

The following methods were discussed.

- Method based on measured c_n and c_t (Inverse b.e.m. method).
  This method is proposed in [34] and [32]. In the start of the project the method has been used by DUT, but in a later stage DUT determined the angle of attack differently, see section 5.2.2. In all Annex XIV experiments, the normal and tangential force on a blade section is measured. Assuming that these forces are uniform over an annular ring, the wake induced velocities can be derived according to the momentum theory (or if necessary from a turbulent wake state model). Since the free stream wind speed and the rotational velocity are known, this yields the effective velocity vector ($\overline{W}$), and consequently the angle of attack ($\alpha_{0,\mathrm{rot}}$).
- Method based on wind tunnel measurements (windtunnel method).
  This method is used by NREL, [35], see also section 4.3.3. A 2D scale model of the blade profile with a flow sensor 0.8 c ahead of the section is placed in a windtunnel. The angle of attack ($\alpha_{0,\mathrm{stat}}$) is known and the local inflow angle ($\alpha_{\mathrm{local,stat}}$) is measured with the flow sensor. Then the angle induced by the bound vorticity is calculated as the difference of both angles (see equation 5.1):

  $$\alpha_{\mathrm{bound,stat}} = \alpha_{\mathrm{local,stat}} - \alpha_{0,\mathrm{stat}} \tag{5.3}$$

  This correction is applied to the measured inflow angle with a similar device under rotating conditions:

  $$\alpha_{0,\mathrm{rot}} = \alpha_{\mathrm{local,rot}} - \alpha_{\mathrm{bound,stat}} \tag{5.4}$$

- Method based on position of stagnation point (stagnation method)
  The method is described in [36]. From the position of the stagnation point (which is obtained from the discrete measured pressure distribution) and the intersection point on the chord a stagnation angle is derived which is an estimate for the angle of attack. The position of the intersection point is determined with the 2D profile design code XFOIL, [37]. Then the position of the intersection point appears to be a weak function of the angle of attack and Reynolds number. Therefore it is assumed that the position of the intersection point depends on the profile geometry only.
  In the sequel two stagnation methods are introduced:
  1. The stagnation (XFOIL) method: The position of the intersection point is determined with a 2D profile code (XFOIL in the present situation).
  2. The stagnation (windtunnel) method: The position of the intersection point is determined from 2D wind tunnel measurements.

  Note that in the ideal situation both methods yield the same result, because they are based on the 'real' 2D stagnation point.
  The ECN method described in [36] can be considered as a combination of the two stagnation methods: The XFOIL stagnation point behaviour is corrected with empirical expressions. These empirical expressions have been obtained from wind tunnel measurements.
- Method based on measured power curve (power method)
  The method is used by Risø and described in [27], see also section 4.4.4. The method results in a correction which should be applied to the measured $\alpha_{local,rot}$. Thereto the power curve is calculated with the blade element momentum theory as function of the angle of attack at a certain spanwise position. The calculated power curve is compared with the measured power curve which is presented as function of the measured inflow angle ($\alpha_{local,rot}$) at the same position. There appears to be a good agreement between both curves if a constant correction to the measured inflow angle is applied.

- Method based on vortex wake calculations
  It is possible to calculate the flow field around the turbine with a 3D panel method, or a simplification of such a model (i.e. a lifting line method). The method yields the vorticity of the rotor blades and the wake. Then the angle induced by the bound vorticity along the blade ($\alpha_{\mathrm{bound,rot}}$) is determined. This angle is used to correct the local inflow angle ($\alpha_{\mathrm{local,rot}}$). In addition a panel method yields the normal force on every blade panel.
  A more simplified wake model is applied by DUT. The DUT method is described in section 5.2.2.

5.2.2 DUT investigation

In [30] the angle of attack for the DUT experiments has been determined with 4 methods:

- Inverse b.e.m. method.
- Angle of attack from the stagnation method.
- Angle of attack from a three hole probe.
  A theoretical upwash correction has been applied. The two dimensional upwash (assuming an infinite untwisted, untapered blade) is calculated using the Schlichting-Truckenbrodt correction, which is described in [38].
  A correction for finite span has been added. This correction is calculated by K. Brown [39].
  Note that the DUT blade is untwisted and untapered. Hence no corrections for twist and taper had to be introduced.
- Angle of attack from two pressure taps.
  The angle of attack was derived directly from two blade pressure taps. The two taps were considered as a built-in flow direction probe.

5.2.3 NREL investigations

In [24] a number of methods to determine the a.o.a. have been introduced.

- Analytic model.
  This method is basically similar to the inverse b.e.m. method, described above.
- Stagnation point normalization (Not to be confused with the stagnation methods described above). If the dynamic pressure is known (see section 6), the resultant inflow velocity can be determined. Then the angle of attack can iteratively be solved from the blade element geometrical relations.
- Pressure profile comparison.
  The static pressure profiles, obtained in a wind tunnel at different angles of attack are compared with the profiles measured on a rotating blade. The angle of attack corresponding to the wind tunnel profile which correlates most highly with the rotating profile was assigned to the rotating data. This method shows some similarity with the stagnation methods in which the stagnation pressures are compared. However, in the present method the complete pressure distribution is compared.

In addition NREL has attempted to apply the stagnation wind tunnel method, see [8].

5.2.4 ECN and RISØ investigations

In addition to the studies described above, ECN and RISØ performed investigation which relate to the angle of attack. The ECN investigation was carried out in the

the EU JOULE projects 'Dynamic Stall and 3D effects' and 'StallVib', [40] and [41]. ECN compared the angle of attack which result from the stagnation point method and from the velocity probe which is located near the 30% station. Note that the angle of attack from the velocity probe was not corrected for upwash effects. The results are discussed in section 5.3.4.

The RISØ investigations concern wind tunnel measurements on the same blade as used for the wind turbine measurements and a comparison between the measured angle of attack and the angle of attack from a full field three dimensional turbulence model. The results are presented in section 5.3.5.

5.3 Evaluation of methods

5.3.1 IEA Annex XIV investigation

The angles of attack from the inverse b.e.m. method, the power method and the stagnation methods were compared with the NREL angle of attack on basis of two NREL time series, one below rated wind speed, the other above rated wind speed. The aim of this study was to obtain insight in the effect of the different angle of attack methods applied in the IEA Annex XIV project. This will be helpful when measurements from different participants are compared mutually. The results are presented in Appendix H

The main conclusion are

- At low angles of attack, most methods agree very well in terms of mean values (disagreement < 1 degrees). For high angles of attack the differences in mean values are in the order of 4 degrees.
- The power method yields angles of attack which differ more from the NREL angle of attack.
- At high angles of attack, the stagnation methods could not be used for the NREL S809 profile due to the fact that in stall the stagnation point is no unique function of the angle of attack. This was also found in the NREL study presented in [8]. Under these conditions, the stagnation (windtunnel) method does not yield a solution at all. Furthermore the stagnation point under rotations remains rather close to the leading edge. This results in relatively small values of the angle even at high wind speeds near the root section.
- Although generally the differences in mean values were considered to be acceptabel the mutual differences in the standard deviation of the angles of attack was often in the order of 50%.

5.3.2 NREL investigation

In [24] the analytic model (i.e. the inverse b.e.m. method), the stagnation pressure profile normalisation technique and the pressure profile comparison technique are compared with the NREL measured angle of attack for a number of campaigns. Note that in these investigations effects of yaw, tower and wind shear have been included. In a separate study NREL applied the stagnation wind tunnel method.

The conclusions from this NREL study were very similar to the conclusions from the IEA Annex XIV study.

- The best agreement with the NREL measured a.o.a.'s was found for the inverse b.e.m. angle of attack. However the frequency resolution of the inverse b.e.m. method is obviously poorer than for the other methods.

- The pressure profile comparison technique (to some extent comparable with the stagnation methods) gave, generally speaking, only a moderate agreement with the NREL a.o.a.
- The stagnation(windtunnel) method could not be applied for high angles of attack.
- The results from the stagnation pressure normalisation agreed reasonably with the NREL measured a.o.a's.
- Some confidence in the NREL measurements for angles of attack at low angles of attack is found from the fact that for these conditions, the NREL rotating measurements give $c_n - \alpha$ curves which agree well with the wind tunnel measurements. This turned out to be true for the twisted as well as the untwisted blade. The $c_n - \alpha$ curves are presented in Appendix E.

5.3.3 DUT investigation

In [30], the results from the methods presented in 5.2.2 are compared with 2D wind tunnel data.

DUT finds a rather large spread in the rotating $c_n - \alpha$ curve, obtained from an inverse bem method. Two explanations are offered:

- The lack of correlation between the measured wind speed upstream of the turbine and the wind speed at the rotor. This however is not consistant with the good results from the inverse b.e.m method described in the previous section.
- Only one sample per revolution is considered, and this sample is assumed to be representative for the complete revolution.

The probe method, the stagnation method and the 'two tap' method give a good agreement with wind tunnel data.

The measurements which are supplied by DUT in the present project have been obtained from the three hole probe with a 2D upwash correction according to Schlichting-Truckenbrodt, see 5.2.2. Furthermore, the correction for finite span according to [39] has been applied, but this correction turned out to be very limited, although for the root station, this correction becomes more important. With the angle of attack, obtained in this way a rotating $c_n - \alpha$ curve is found which for low angles of attack agree well with the wind tunnel measurements.

The 2D upwash correction method has been assessed by reproducing the NREL upwash wind tunnel measurements. An excellent agreement was found (differences < 2 degrees until α = 20 degrees, increasing to 4 degrees at α = 30 degrees).

In order to compare the data in the Annex XIV base mutually, is important to know the effect of manipulations of the angle of attack carried out by the different participants. Although the DUT method was not included in the IEA Annex XIV study or the NREL studies from the sections 5.3.1 or 5.3.2, the good agreement between the DUT calculation and the windtunnel measurement of upwash for the NREL blade, leads to the conclusion that the angles of attack obtained with the DUT method would have given very similar results to the NREL measured angles of attack.

5.3.4 ECN investigation

Within the EU JOULE projects 'Dynamic Stall and 3D effects' and 'StallVib', [40] and [41], ECN carried out two investigations.

The first comparison was based on averages and standard deviations of angles of attack α and inflow velocities W [40, section 3.3.5]. To this end the measurement 'ny_rot_e_003' was selected because both the stagnation point and the velocity probe method were applied in their calibration range here. By comparing measured angles of attack to 'geometric' angles of attack it was found that the stagnation angles correspond better to the geometric angles of attack than the probe angle of attack. This analysis of averages and standard deviations led to the conclusion a stagnation angle is the better estimate to the angle of attack.

With regard to the comparison on basis of averaged values it must be emphasized that the comparison is made with the 'geometric' angle of attack, not taking into account the effect of the wake induced velocity. Furthermore an upwash correction was not included in the probe angle of attack. Both these effects may influence the average value considerably.

The second comparison consisted of determining correlation and phase of the normal force coefficient c_n and the angle of attack α [41, section 2.6], where c_n and α were measured at the 30% station according to the stagnation point method and α was measured at the 35% station according to the velocity probe method. Also the 'stagnation angles' at the other stations at all stations were considered. As a test case the measurement 'ny_rot_e_001' was selected because for the 30% station the normal force coefficient is in the linear region. This analysis of correlation and phase led to the conclusion a stagnation angle is a better estimate to α than a probe angle of attack because it is better correlated to the normal force coefficient. The α signal from the 30% station however has too low an auto-correlation to be of use in time series analysis (in contrast to the α signals from the 60% and the 80% station).

5.3.5 RISØ investigation

In 1993 wind tunnel measurements were performed on the same blade as used for the wind turbine measurements [42]. The blade including the five hole pitot tube was placed in a 4x4 m jet in a wind tunnel facility in Jutland, Denmark. The jet was centred around the mid blade segment of the blade with the pitot tube in position 5 just outboard of the section and thus in the same position as used during the measurements on the turbine. Measurements were performed at a wind speed around 30 m/s and the angle of attack measurement from the pitot tube was compared with a measurement of the blade pitch which can be considered as the geometrical angle of attack. The comparison is presented in figure 5.3. As in the field rotor measurements no correction for upwash was introduced but it is seen that a good correlation is found in most of the considered interval with the biggest deviations at low angle of attack. The reason for a good correlation without a correction for upwash is that in this case as well as on the rotor the flow field is influenced by both upwash from the bound circulation around the blade and downwash from the shed vorticity due to the variation of the bound circulation along the blade span.

In another project [43] the statistical properties of the measured angle of attack and has been compared with simulations of the inflow to the blade using a full field three-dimensional turbulence model. The power spectral density function of the angle of attack compared for the measurements and the simulations in figure 5.4. In general a good correlation is found in the frequency interval up to 3P which is around 2.5 Hz.

Figure 5.3 *Comparison of the blade pitch angle and the angle of attack measured with the pitot tube during a wind tunnel experiment*

5.4 Conclusion on angle of attack methods

- From the investigations described in this section it is expected that, below stall the mutual differences in mean angles of attack will be in the order of 1 degree. Above stall, the agreement in mean values will be worse and in the order of 4 degrees.
- The mutual differences in the standard deviations of the angles of attack obtained with the different methods can be in the order of 50%.
- The frequency resolution of the inverse b.e.m. method is probably too poor for dynamic stall investigations.
- For the NREL S809 profile, the stagnation method cannot be used at high angles of attack.
- Most comparisons which have been made rely on time averaged data, Auto Power Spectral Densities and standard deviations. This implies that a possible phase lag is not considered. For example in the inverse b.e.m. method the wind speed is measured some distance from the turbine. This may introduce a phase lag. The same holds for the methods which rely on inflow angle measurements with a flow device. These devices are located a certain distance from the pressure taps in order to avoid flow distortion. The ECN investigation described in section 5.3.4 indicates that this effect may be significant.
- Most turbines which have been used for the investigation had untwisted and untapered blades. If twist and taper are taken into account, the discrepancies may become larger. However it must be noted that under rotating conditions it is not necessarily true that an untwisted and untapered blade is 'more' 2-dimensional than a twisted and tapered blade: The twist of the blade will compensate the effect of rotation and hence the loading along the blade will be more or less constant for a twisted blade.

Figure 5.4 *Comparison of the power spectral density function of the angle of attack; measured with the pitot tube and simulated with an aeroelastic model including a three-dimensional turbulence model, respectively*

There are two indications (no evidence!) that the twist effect and the finite span has a limited effect on the upwash:

1. The $\mathrm{cl} - \alpha$ curve for the NREL twisted and untwisted blade are similar, using the same wind tunnel 2D upwash correction, see [8]! This implies that the disturbance of twist on the upwash correction is limited.
2. The results presented in 5.3.3 indicate that also the finite span has limited effect on the the upwash.

The RISØ investigation however indicates that there is an important effect from the variation of the bound vorticity along the blade. The shed vorticity which results from this variation yields an upwash which compensates the 2D upwash for the bound circulation.

- The good mutual agreement in mean angles of attack does not necessarily mean that the methods give accurate results. The main problem is the fact that the angle of attack which result from the different methods cannot be compared with the 'real' angle of attack, because the 'real' angle of attack according to the description from section 5.1 is a hypothetical quantity which is never known.

6. DYNAMIC PRESSURE AND NON-DIMENSIONALISATION IN FIELD EXPERIMENTS

6.1 General

The measured data which are considered in the IEA Annex XIV project are usually presented as coefficients which are non-dimensionalised with the dynamic pressure.

In a wind tunnel environment the value of the dynamic pressure can be obtained from the tunnel speed.

In a rotating environment, the dynamic pressure should be obtained from the local wind speed at the profile. This local wind speed cannot be derived straightforward from the free stream wind velocity and the rotational speed due to the presence of the wake induced velocities u_i and u_t. A comparison between three different methods for obtaining the dynamic pressure is reported in [24]. The results are discussed below.

Another problem is introduced by the fact the pressures are measured as differentials relative to an (unknown) reference pressure, see section 4. Hence the absolute pressures are unknown. This holds for the pressure tap measurements of DUT, ECN, NREL and IC/RAL and for the stagnation pressure measurements in all experiments (including the RISØ test).

As explained in section 4, most participants obtain the aerodynamic forces on a blade profile from integration of the pressure profile. The integration can generally be written as the difference of two integrations. For example the integration of the normal force is split into an integration over the suction side and over the pressure side. In general form the equations can be written as

$$f_{aero} = \int_{side1} (p_{side1} - p_{ref}) \cdot ds_{side1} - \int_{side2} (p_{side2} - p_{ref}) \cdot ds_{side2} \qquad (6.1)$$

Note that the pressure profiles and the reference pressure may be corrected for centrifugal forces or other phenomena. In the present discussion these corrections do not need to be adressed: The effect of the unknown reference pressure is analysed only qualitatively.

Now it may be assumed that all measurement systems in the present project are sufficiently fast, to assume that the reference pressure is approximately constant during the recording of the pressure profile around the section. Then the aerodynamic forces are obtained from:

$$f_{aero} = \int_{side1} p_{side1} \cdot ds_{side1} - \int_{side2} p_{side2} \cdot ds_{side2} \qquad (6.2)$$

Hence the reference pressure does not appear in the derivation of the aerodynamic forces and consequently the absolute value of the aerodynamic forces are not obscured by the unknown reference pressure (This is obviously also true for the RISØ experiments, where the aerodynamic forces are obtained from balance measurements).

The dynamic pressure is usually derived from probe measurements or from the maximum in the pressure distribution, see also section 6.2.

$$q = p_{pitot} - p_{ref} \tag{6.3}$$

or:

$$q = p_{max} - p_{ref} \tag{6.4}$$

Note that this gives rise to a systematic difference with respect to the wind tunnel coefficients, where the dynamic pressure is related to a static pressure. Such equivalent static pressure at a wind turbine does not exist.

An additional uncertainty from the reference pressure is introduced into the pressure coefficient. In the wind tunnel environment the pressure coefficient is defined as:

$$C_p = \frac{p_{tap} - p_\infty}{q} \tag{6.5}$$

With p_∞ the static pressure. In the field experiments, the pressure coefficient is obtained from:

$$C_p = \frac{p_{tap} - p_{ref}}{q} \tag{6.6}$$

As stated above, the denominator (q) is influenced by the reference pressure, but now the numerator is influenced too.

With regard to this subject, much discussion took place within the IEA Annex XIV group in particular on the harmonic ripple observed in the DUT experiments, see section 4.5.5. In the DUT measurements the reference pressure is stabilised by means of a damper, which causes the C_p to vary harmonically with the altitude. However until now, no such effect is observed in the measurements from the other institutes.

6.2 Methods available to determine the dynamic pressure

In [24] three different methods are introduced to obtain the dynamic pressure.

1. An analytic model.
   The local velocity components, and hence the dynamic pressure at each primary span location, were estimated from the geometry of the inflow relative to the turbine. The profile of the tower shadow velocity deficit was modeled using a cosine function. A b.e.m. code (PROP) was used to predict axial induction factors at each of the primary span locations over a range of wind speeds. The axial induction factors were adjusted for wake deformation under yawed conditions using a skewed wake correction. Only measured values of azimuth angle, yaw angle, and upwind wind speed were used. Then it is important to note that the dynamic pressure obtained from this method is <u>not</u> obscured by the uncertainty in reference pressure.
2. A stagnation pressure normalisation: The maximum positive value in the discrete pressure distribution is searched for. If necessary a curve fit is applied around the maximum, but this does not fundamentally change the method. Note that the maximum in the pressure distribution is measured relative to the reference pressure. The dynamic pressure is obtained from equation 6.4
3. A method in which the dynamic pressure is obtained from a pitot pressure probe.
   The pitot pressure is measured relative to the reference pressure. The dynamic pressure is obtained from equation 6.3.

6.3 Evaluation of methods

In [24], NREL compared the results of the methods presented in section 6.2 for several campaigns. It is found that the stagnation pressure normalisation methods yield dynamic pressures very closely to the probe dynamic pressures, despite the fact that the probes are placed some distance from the pressure taps. In contrast to this observation ECN concluded within the EU JOULE project 'StallVib' that the inflow velocity obtained with the stagnation method was a better estimate than a probe velocity, [41].

Although in [24], the dynamic pressures from the analytic model show a less good agreement with the measured dynamic pressures, the agreement is acceptable and the differences can probably be attributed to b.e.m. model deficiencies. This implies that the uncertainty in reference pressure has no severe consequences on the dynamic pressure.

In the RISØ investigation described in [43] the measured relative velocity was compared with simulations of the inflow to the blade using an advanced analytic model, i.e. a full field three-dimensional turbulence model. The power spectral density function of the angle of attack is compared for the measurements and the simulations in figure 6.1. In general a good correlation is found in the frequency

Figure 6.1 *Comparison of the power spectral density function of the angle of attack; measured with the pitot tube and simulated with an aeroelastic model including a three-dimensional turbulence model, respectively*

interval up to 3P which is around 2.5 Hz.

6.4 Conclusion on non-dimensionalisation of coefficients

A very encouraging result is that generally all methods which are used in the IEA Annex XIV project to determine the dynamic pressure, yield a good mutual agreement.

The reasonable agreement between the analytic models (which are not influenced by the unknown reference pressure) and the other methods indicates that the

uncertainty from the reference pressure on the aerodynamic coefficients may be limited.

It must be noted however that only a limited number of experimental facilities were considered in the studies and a more thorough investigation on the differences in dynamic pressure methods from the participants is required.

7. DESCRIPTION OF DATABASE

7.1 Conventions and notations

The prescribed definition of conventions and notations are given in Appendix A.

7.2 Format of the files, filetypes and filenames

In order to facilate the selection of signals from a file, it was considered essential that all files were supplied in the same format. It was agreed that three types of files had to be supplied:

1. Log files. These files contain general information about the measurement procedure. It should also contain:
   - date and time of measurement
   - air density, pressure and temperature
   - information which is needed to read the other files (like the number of pressure taps, the number of anemometers, etc.)
2. Profile files. These files contain the wind speeds, the wind directions, the rotor speed, the pitch angle, the mechanical loads, the angles of attack and the inflow velocities, the profile coefficients (c_n, c_t and c_m) all as f(t,ϕ_r).
3. Pressure files. These files contain the pressure recordings.

The format of the files is specified. The files start with the statistics (mean, max, min, standard deviation) of every signal.

The filenames are structured as follows:
'(n)y_ext1_ext2_ext3_n'

- (n)y refers to (non)-yawed conditions;
- ext1 refers to the file type:
  - log = log file
  - prof = file with wind conditions and profile data;
  - p1—-pN = files with pressures
- ext2 refers to the type of experiment:
  - rot = rotating conditions
  - non = non-rotating conditions
  - slow = slowly rotating conditions (not supplied in the present project)
- ext3 refers to the name of the participant:
  - d = DUT
  - e = ECN
  - i = IC/RAL
  - nu = NREL untwisted blade, phase II (section 4.3)
  - nt = NREL twisted blade, phase III (section 4.3)
  - ntp = NREL twisted blade, phase IV (section 4.3)
  - r = RISØ
- n is the unique label of the experiment

For example ny_p03_rot_nt_001 is the first NREL datafile of phase III which contains the pressure data of the 3rd blade section obtained for non yawed conditions.

Actually the filenames may be abbreviated in case the operating system allows only a limited number of characters for the filename, see also section 7.4.

7.3 Content of database

A total of more than 125 files with a length of $\approx$ 10000 s have been stored into the database. The length of the time series range between 15s and 10 minutes. Data over a 10 minute period could be supplied by Risø, because this institute measured the aerodynamic forces only. The other participants also supplied pressure files. Then measurements from a shorter time period had to be supplied in order to limit the amount of data.

Rotating as well as non-rotating experiments are stored. Furthermore the measurements are supplied for non-yawed and yawed conditions. NREL has supplied measurements of the Phase II, III and IV experiments.

The angle of attack varies between negative values and deep stall. The adjustment of angle of attack is realized in different ways by the participants:

- By means of a variation in wind speed; This has been realized by ECN, RISØ, IC/RAL and NREL
- By means of a variation in rotor speed. This has been realized by DUT and ECN
- By means of a variation in pitch angle: This has been realized by ECN

A list of content of the base is annexed in Appendix B.

7.4 Electronic medium

The database is stored on CD-ROM and on a public ECN ftp site. The ftp site can be reached by anonymous ftp at the following adress: $ftp.ecn.nl$, directory $/pub/de/IEAXIV/data$.

In order to limit the required disc capacity, the files are compressed by means of the zip utility. A utility to unzip the files is added to the database at directory $/pub/de/IEAXIV/utils$. At the ftp site, some abbreviation of the file names took place in order to make the length of the file name MS-DOS compatible. It is expected that the abbreviated file names are self-explanatory, however key files which translate the MS-DOS conventions to the prescribed conventions are available too.

8. CONCLUSIONS, LIMITATIONS AND RECOMMENDATIONS

8.1 Conclusions from IEA Annex XIV

The objective of IEA Annex XIV was to collaborate in performing full scale aerodynamic test programs and to create a data base of aerodynamic measurements. After more than 4 years of close cooperation between institutes performing such experiments the objective was met:

- A unique database has been developed in which detailed aerodynamic measurements are stored. A total of about 125 time series of aerodynamic field measurements is available.
  - The measurements are obtained on 5 different wind turbines: The diameter of these turbines ranges from 10 to 27 m. Very different blades have been considered:
    - Blades without twist and taper;
    - A blade with twist but without taper;
    - Blades with twist and taper;
  - Measurements have been supplied for very different conditions, including yaw misalignment. The angles of attack range between negative values and deep stall. The angle of attack has been varied by means of a variation in wind speed but also by means of pitch angle and rotor speed.
  - All parties have provided :
    - An aeroelastic model description to aid in the interpretation of the measurements;
    - Measurements of ambient conditions
    - Measurements of operational conditions
    - Measurements of global blade and rotor data (i.e. blade loads)
    - Measurements of local aerodynamic forces and inflow conditions.
- The access to the database is made as easy as possible. Thereto the files are stored in a uniform format. In addition, the conventions which have been applied in the database are uniform and the file names are prescribed. Furthermore, the database is documented and statistical overviews are supplied for every file, which will assist the user to select relevant data.
- The data are accessable on a public ftp site at ECN, which can be reached by anonymous ftp at adress $ftp.ecn.nl$ at directory $pub/de/IEAXIV$. In addition the data are stored on CD-ROM (available at ECN under reference ECN-CD–97-019).
- In interpreting the measurements and when comparing field data with wind tunnel experiments it should be kept in mind that the definition of angle of attack, dynamic pressure and aerodynamic coefficients is less straightforward than in the wind tunnel case. Several methods are applied by the IEA Annex XIV participants for the determination of these quantities. A number of investigations were performed on behalf of Annex XIV or by the participants independantly which addressed the problem of angle of attack, dynamic pressure and aerodynamic coefficients:
  - In general, no conclusion could be drawn about the accuracy of the methods because no values for the 'real' angles of attack and dynamic pressure were

available to compare with;

– A mutual comparison of results and a comparison with non-rotating wind tunnel data (from DUT and NREL) has led to the following indications:
  * The mutual agreement between the mean angles of attack from the different methods was good (in the order of 1 to 4 degrees). However in terms of standard deviation, the differences were in the order of 50%.
  * The mutual agreement between the dynamic pressure from the different methods was good;
  * Although the unkown reference pressure can introduce uncertainties in the aerodynamic coefficients, the introduction of a method which did not suffer from this problem indicated that this uncertainty is limited.

  It must be noted that the above mentioned indications are still premature and mainly based on analysis and measurements of turbines with untwisted untapered blade. More investigation is required in order to draw more thorough conclusions.

8.2 Benefits from IEA Annex XIV

The main benefits from IEA Annex XIV are:

- A huge amount of local aerodynamic measurements has become available, which are stored into a well documented database. It is expected that the database will serve as validation base for the development and validation of aerodynamic models. The supply of local aerodynamic data, is a major step forward in understanding the aerodynamic behaviour of a wind turbine: In conventional experimental programs only integrated blade (or rotor) quantities are measured from which the local aerodynamic properties can be derived only indirectly.
- The IEA Annex XIV served as a platform where very specific knowledge associated with aerodynamic measurements could be exchanged. All participants agree that this has been very instructive and enabled the acceleration of the experimental programs.

8.3 Limitations of measurements in IEA Annex XIV database

In applying the results from the database one should realize the limitations of the experimental data. Several uncertainties need to be considered:

- Uncertainties introduced by the instrumentation, including calibrations. These uncertainties are believed to be limited. An exception may be the measurements at standstill which result in very low pressure levels and a poor accuracy.
- Uncertainties due to 'definition' problems of angle of attack, dynamic pressure and aerodynamic coefficients. The participants have manipulated these data in different ways.
- Uncertainties which originate from the (partly) unknown inflow conditions. These uncertainties are inevitible in view of the highly turbulent environment in which the wind turbine operates.
- The length of some time series may be too short for some investigations.

Apart from this there is an uncertainty from the aeroelastic model descriptions: In the interpretation of data the aeroelastic model description will be essential but it is known that some data from the model descriptions suffer from uncertainties whereas other data are not available.

8.4 Recommendations from IEA Annex XIV

- Within IEA Annex XIV much effort had to spent on the exact definition of wind turbine conventions, notations and reference systems. This item was essential in the present project where data from different institutes had to be harmonized. This implied that the participants had to reprocess their datafiles and several data exchange rounds appeared to be necessary before all participants supplied the measurements according to the common specifications. It is recommended that the wind energy society should reach consensus about common conventions, definitions, notations and reference systems.
- The uncertainty which results from the definition problem of angle of attack, dynamic pressure and aerodynamic coefficients is still too large. More research on this field is required.
- The maximum rotor diameter in the present project was 27 m. Although at the start of the project, this was considered to be a medium sized turbine, the trend has been toward much larger machines and at the end of the project the turbine was regarded as a relatively small turbine. It is recommended to proceed with experimental programs on larger scale wind turbines.
- Although much effort was spent on the harmonisation of the file formats, some differences in file formats are inevatible. This is mainly due to the differences in experimentation. This results in a different number of measurement signals and consequently different file formats. Even these slight differences in file format make it necessary that the user has to spent much effort on analysing the various file formats. Due to the large file sizes this is a time consuming task. This can be avoided by making a user friendly computer program from which the data can easily be extracted from the data base.
- It is recommended to maintain the database. By maintaining the database an extensive use of the database can be expected, not only in the near future, but also on the long term:
  - The database is created using the most recent state of knowledge. It would be very beneficial if new insights which are to be expected in the future could be included in the database. For example: It is possible that new wind tunnel calibration experiments or CFD calculations will be performed from which angles of attack can be updated. It is emphasised that this is a relatively easy task because the raw measurements are still available at every participant. This implies that there is no need to collect new measurements if the postprocessing should be performed in a different way.
  - It is recommended to store 2D wind tunnel measurements on the blade sections into the database. These measurements can serve as reference for the full scale measurements and can aid in the interpretation of the full scale measurements.
  - The purpose of the present project was to create a data base, not to utilize the base. It is anticipated that after using the database recommendations can be defined, on how to fill the 'gaps' in the database.
  - Most of the experimental facilities are still operational. Several very useful measurements are still expected:
    - IC/RAL has only supplied a limited number of datafiles. More files are to be expected in the future;
    - DUT has only supplied measurements of the 70% section. Measurement from the 50% and 30% station are expected in the near future.
    - Several institutes will perform measurements using boundary layer manipulators. At present, no such measurements are included in the base.

The storage of these data will definitely improve the quality of the database.

REFERENCES

[1] H. Snel and J.G Schepers (ed.) . "JOULE1: Joint investigation of Dynamic Inflow Effects and Implementation of an Engineering Method". ECN-C-94-107, December 1994.

[2] A. Björck. "Dynamic Stall and Three Dimensional Effect ". FFA-TN –1995-31, FFA, 1995.

[3] J.G. Schepers. "Minutes of the preparatory meeting of the IEA Annex 'Field Rotor Aerodynamics' held at the University of Delft on December 2nd, 1992". DE-Memo- 92-79, ECN, December 1992.

[4] J.G. Schepers. "Minutes of the first meeting of the IEA Annex 'Field Rotor Aerodynamics' held at Risø National Lab. (DK) on September 16th and 17th, 1993". DE-Memo- 93-72, ECN, September 1993.

[5] J.G. Schepers. "Minutes of the second meeting of the IEA Annex 'Field Rotor Aerodynamics' held at the Technical University of Delft (NL) on March 17th and 18th, 1994". DE-Memo- 94-28, ECN, March 1994.

[6] J.G. Schepers. "Minutes of the third meeting of the IEA Annex 'Field Rotor Aerodynamics' held at Rutherford Appleton Laboratory (UK) on April 5th , 1995". DE-Memo- 95-23, ECN, March 1995.

[7] J.G. Schepers. "Minutes of the fourth meeting of the IEA Annex 'Field Rotor Aerodynamics' held at National Renewable Energy Laboratory (USA) on February 5th and 6th , 1996". DE-Memo- 96-13, ECN, February 1996.

[8] J.G. Schepers. "Minutes of the fifth meeting of the IEA Annex 'Field Rotor Aerodynamics' held at Netherlands Energy Research Foundation (NL) on June 14th, 1996". DE-Memo- 96-41, ECN, July 1996.

[9] A.J. Brand J.W.M. Dekker C.M. de Groot and M. Spath. "Overview of aerodynamic measurements on an Aerpac 25 WPX wind turbine blade at the HAT 25 experimental wind turbie ". ECN-DE-Memo--96-014, ECN, 1996.

[10] M. Späth. "Implementation of a pressure scanner system for a field rotor aerodynamics experiments ". ECN-R –93-017, ECN, 1993.

[11] M. Späth and N. Stefanatos. "Survey on frequency responses of pressure tubes installed in a 12.5 meter rotor blade ". ECN-I –92-028, ECN, September 1992.

[12] A.J. Brand. "Specifications for a spheric velocity probe ". ECN-CX –93-133, ECN, November 1993.

[13] A.J. Brand G.P. Corten and M. Späth. "Calibration and measuring procedure of a spheric velocity probe ". ECN-R –95-031, ECN, February 1996.

[14] D.W. Brye and R.C. Pankhurs. *"Pressure probe methods for determining wind speed and flow direction"*. HMSO, 1971.

[15] C.P. Butterfield et al. 'Combined Experiment PHASE I, final report". NREL TP- 257-4655, October 1992.

[16] D. Somers. "Design and Experimental Results for the S809 Airfoil", NREL/TP-442-6918, unpublished.

[17] D.A. Simms L.J. Fingersh and C.P. Butterfield. "NREL Unsteady Aerodynamics Experiment Phase III Test Objectives and Preliminary Results.". In *ASME/ETCE Conference, Houston, USA*, January 1995.

[18] L.J. Fingersh and M.C. Robinson. "Wind Tunnel Calibration of 5-hole Pressure Probes for Application to Wind Turbines". In *ASME Wind Energy Symposium, Reno USA*, January 1997.

[19] D.A. Simms and C.P. Butterfield. "PC-Based PCM Telemetry Data Reduction System Hardware.,"SERI/TP-257-3662, 1990.

[20] D.A. Simms and C.P. Butterfield. "A PC-Based Telemetry System for

Acquiring and Reducing Data from Multiple PCM Streams. ”SERI/TP-257-4123, 1991.

[21] M.S. Miller et al. “Determination of Data Reliability for Phase II of the Combined Experiment,” NREL unpublished.

[22] B. McNiff and D.A. Simms. “Error Analysis in Wind Turbine Field Testing”. In *Windpower ’92 Proceedings, Seattle, USA*, October 22-23 1992.

[23] S.A. Huyer D.A. Simms and M.C. Robinson. “Unsteady Aerodynamics Associated with a Horizontal-Axis Wind Turbine”. *American Institute of Aeronautics and Astronautics Journal, Volume 34, No. 10.*, July-Sept. 1996.

[24] D.E. Shipley et al. ‘Techniques for the determination of local dynamic pressure and angle of attack on a horizontal axis wind turbine blade”. NREL TP- 442-7393, May 1995.

[25] A. Pope and J.J. Harper. *“Low speed Wind Tunnel Testing”*. New York, John Wiley and Sons, 1966.

[26] D.A. Simms M.C. Robinson M.M. Hand and L.J. Fingersh. “Characterization and Comparison of Baseline Aerodynamic Performance of Optimally-Twisted Versus Non-Twisted HAWT Blades”, Prepared for 15th ASME Wind Energy Symposium, NREL/TP-442-20281, January 1996.

[27] H.A. Madsen. ‘Aerodynamics of a Horizontal-Axis Wind Turbine in Natural Conditions”. Risø M-2903, Risø National Laboratory, September 1991.

[28] H.A. Madsen. ‘Aerodynamics of a Horizontal-Axis Wind Turbine in Natural Conditions- Raw data overview”. Risø M-2902, Risø National Laboratory, September 1991.

[29] H.A. Madsen. “Structural Dynamics of a 100 kW HAWT”. Risø M-2887, Risø National Laboratory, February 1991.

[30] A. Bruining . “Aerodynamics characteristics of a 10 m diameter rotating wind turbine blade, ” University of Delft, IW-084R, September 1996.

[31] G.P. Corten. “Accuracy Analysis of Field Pressure Measurements, perspective for future measurements ” Delft University of Technology, DUT-IvW-95085R, June 1995.

[32] A. Bruining G.J.W. van Bussel C.P. Corten and W.A. Timmer. “Pressure distributions from a wind turbine blade; field measurements compared to 2-dimensional wind tunnel data ”. DUT-IvW- 93065R, Delft University of Technology, August 1993.

[33] J.G. Schepers. “Calculation of induced velocities upstream of the WPS-30 turbine”, ECN, February 1992.

[34] H. Snel, R. Houwink and Bosschers J. “Sectional prediction of lift coefficients on rotating wind turbine blades in stall ”. ECN-C –93-052, ECN, May 1993.

[35] C.P. Butterfield. “Three-dimensional airfoil performance measurements on a rotating wing”. In *Proceedings of EWEC Conference, Glasgow, 10-13 July 1989*, July 1989.

[36] A.J. Brand. “To estimate the angle of attack of an airfoil from the pressure distribution ”. ECN-R –94-002, ECN, January 1994.

[37] M. Drela. “XFOIL: An analysis and design system for low Reynolds number airfoils”. *Low Reynolds number aerodynamics, Lecture notes in Engineering 54*, 1989.

[38] H. Schlichting and E. Truckenbrodt. “Aerodynamics of the Airplane ” McGraw-Hill, ISBN 0-07-055341-6,, 1979.

[39] K. Brown. “Results 3D free wake panel method, ” University of Bristol (UK), E-mail document to A. Bruining, May 1995.

[40] A.J. Brand J.W.M. Dekker C.M. de Groot and M. Spath. “Aerodynamic field data from the HAT25 experimental wind turbine - Contribution to the EC/NOVEM project ‘Dynamic Stall and Three-dimensional effects ”. ECN-R--96-037, ECN, 1996.

[41] A.J. Brand. “ECN Progress Report Work Package #1 EU STALLVIB project; Actions M-1, M-2 and M-4 ”. DE-Memo-96-045, ECN-Renewable Energy, 1996.

[42] I. Antoniou, H.A. Madsen and F. Rasmussen. “Wind Tunnel Measurements on a LM 8.2 m Blade”. Risø I-800(EN), Risø National Laboratory, December 1995.

[43] A. Kretz, H.A. Madsen and J.T. Petersen. “Measured and Simulated Turbulence - Compared at a Section of a Rotating Wind Turbine Blade”. Risø R-671(EN), Risø National Laboratory, March 1994.

[44] J.G. Schepers and H. Snel (ed.) . “JOULE2: Dynamic Inflow: Yawed Conditions and Partial Span Pitch”. ECN-C-95-056, June 1995.

[45] L.W.M.M Rademakers and P.A. van der Werff. “Verification of wind turbine design codes with the ’Dutch Handbook wind data for wind turbine design’, ECN-I–92-048 ”, December 1992.

[46] H.J.T. Kooijman. “Smart rotor, feasibility study for a passive pitch regulation of a wind turbine rotor blade,” ECN-I-96-011, March 1996.

[47] A.J. Brand. “Aerodynamic Field Data of a Non-Rotating Blade”. ECN-C--95-063, ECN, August 1995.

[48] Lekkerkerk, F.L. "Regelstrategieen van de 25 m HAWT (In Dutch)", ECN-83-120, Juni 1983.

[49] I.H. Abbott and A.E. Doenhoff. *Theory of Wing Sections*. Dover Publications, Inc, 1958.

[50] J.G. Schepers. “PVOPT, Theory and test cases, ” ECN-C–96-057, January 1996.

[51] J.G. Schepers. “GAPHAT – III, Model description and verification (Dutch) ”. ECN -I–91-054, ECN, Juli 1991.